

63-4-2

AFCRL-63-653

CATALOGED BY DDC
AS AD No. 408555



THE PENNSYLVANIA
STATE UNIVERSITY

IONOSPHERIC RESEARCH

Scientific Report No. 189

AN INVESTIGATION OF THE INFLUENCE OF COLLISIONS ON LOW FREQUENCY GROUP HEIGHTS

by

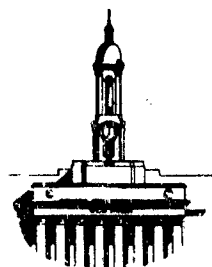
J. D. Hardy

July 15, 1963

*"The research reported in this document has been sponsored
by the Geophysics Research Directorate of the Air Force
Cambridge Research Laboratory, Office of Aerospace Research,
United States Air Force, under Contract AF19(604)-8012."*

408 555

IONOSPHERE RESEARCH LABORATORY



University Park, Pennsylvania

Contract No. AF19(604)-8012
Project 7663, Task 766301

"Requests for additional copies by Agencies of the Department of Defense, their contractors, and other Government agencies should be directed to the:

DEFENSE DOCUMENTATION CENTER
ARLINGTON HALL STATION
ARLINGTON 12, VIRGINIA

Department of Defense contractors must be established for DDC services or have their 'need-to-know' certified by the cognizant military agency of their project or contract."

"All other persons and organizations should apply to the:

U. S. DEPARTMENT OF COMMERCE
OFFICE OF TECHNICAL SERVICES
WASHINGTON 25, D. C."

AFCRL - 63-653

Ionospheric Research
Contract AF19(604)-8012
Scientific Report

on

"An Investigation of the Influence of Collisions
on Low Frequency Group Heights"

by

J. D. Hardy
July 15, 1963

SCIENTIFIC REPORT NO. 189
(Project 7663, Task 766301)

"The research reported in this document has been sponsored by the Geophysics Research Directorate of the Air Force Cambridge Research Laboratory, Office of Aerospace Research, United States Air Force, under Contract AF19(604)-8012."

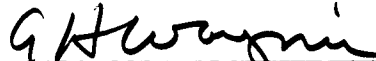
Ionosphere Research Laboratory

Submitted by:



A. J. Ferraro, Assistant Professor
of Electrical Engineering

Approved by:



A. H. Waynick, Professor of
Electrical Engineering, Director IRL

THE PENNSYLVANIA STATE UNIVERSITY
College of Engineering
Department of Electrical Engineering

TABLE OF CONTENTS

| | Page |
|---|------|
| ABSTRACT | 1 |
| LIST OF SYMBOLS | ii |
| 1. INTRODUCTION | 1 |
| 1.1 Origin of the Problem | 1 |
| 1.2 Previous Related Studies | 2 |
| 1.3 General Statement of the Problem | 5 |
| 1.4 Specific Statement of the Problem | 5 |
| 2. MATHEMATICS OF GROUP HEIGHT | 7 |
| 2.1 Full-wave Theory | 7 |
| 2.2 Ray Theory | 9 |
| 2.3 Phase Integral Method | 14 |
| 2.4 The Conversion of h'f Records to N-h Profiles . | 16 |
| 3. THE GROUP INDEX OF REFRACTION INCLUDING COLLISIONS AND MAGNETIC FIELD | 19 |
| 3.1 Appleton-Hartree and μ' Equations | 19 |
| 3.2 Presentation of μ' Curves | 22 |
| 3.3 General Discussion of the Influence of Collisions | 34 |
| 4. INFLUENCE OF COLLISIONS ON GROUP HEIGHTS | 39 |
| 4.1 Method of Obtaining Group Heights | 39 |
| 4.2 Presentation of Tables | 41 |
| 4.3 Importance of Collisions | 52 |

| | | |
|-----|---|----|
| 5. | PRESENTATION OF TYPICAL RECORDS FOR WHICH RAY | |
| | THEORY CAN BE APPLIED | 56 |
| 5.1 | Presentation of Records | 56 |
| 5.2 | Brief Description of the Low Frequency | |
| | Ionosonde | 59 |
| 6. | SUMMARY AND CONCLUSIONS | 63 |
| 6.1 | Statement of the Problem | 63 |
| 6.2 | Review of the Procedure | 63 |
| 6.3 | Conclusions | 64 |
| 6.4 | Suggestions for Further Study | 66 |
| | REFERENCES | 67 |
| | APPENDIX A | 69 |

ABSTRACT

In this report virtual heights from five different models representing realistic ionospheres are computed. Computations are made including collisions and neglecting collisions, and the results are compared to determine the magnitude of the errors produced when collisions are neglected. Limitations are stated which must be placed upon frequency and model shapes, in order that ray theory may be applied.

LIST OF SYMBOLS

$$X = \omega_n^2 / \omega^2$$

$$Y_L = \omega_L / \omega$$

$$Y_T = \omega_T / \omega$$

$$Z = \nu / \omega$$

$$\omega_n^2 = 4 \pi N e^2 / \epsilon_0 m$$

$$\omega_H = \mu_0 e B_0 / m = \text{angular gyro-frequency}$$

$$\omega_L = \frac{\mu_0 e B_0 \cos \theta}{m}$$

$$\omega_T = \frac{\mu_0 e B_0 \sin \theta}{m}$$

e = magnitude of charge of electron in coulombs

m = mass of electron in kg.

ϵ_0 = permittivity of free space

μ_0 = permeability of free space

$k = 2\pi f / c =$ propagation constant in free space

B_0 = magnitude of imposed magnetic field in Weber/m²

N = electron density/m³

N_c = electron density corresponding to the level where
 $X = 1.$

N_y = electron density corresponding to the level where
 $X = 1 + Y$

N_m = electron density at the peak of the layer

ν = collision frequency/sec

ν_c = critical collision frequency

$n = \mu - j\chi =$ phase refractive index

$\mu = c / v_p$

v_p = actual phase velocity

$\mu' = c/v_g$ = group refractive index

v_g = actual group velocity

E_x, E_y, E_z = wave field electric vector components

H_x, H_y, H_z = wave field magnetic vector components

F, F_0, F_x = field variables in Försterling's equations

f = operating frequency (cycles/sec unless otherwise noted)

$f_n = [Ne^2/\pi\epsilon_0 m]^{\frac{1}{2}}$ = plasma frequency

f_p = penetration frequency for the ordinary mode

h = height (km)

$h-f$ = true height

$h'f$ = virtual or group height

h_r = height of reflection

h_b = height of the base of the ionospheric model

h_m = height of maximum electron density

ψ = coupling parameter

ρ = wave polarization

θ = angle between B_0 and the positive z axis

z axis is vertical with positive direction upwards

y axis is horizontal in magnetic north direction

x axis is horizontal in magnetic east direction

Time varying factor $e^{+j\omega t}$ for all wave quantities

1. INTRODUCTION

1.1 Origin of the Problem

Radio sounding by pulsed radio waves is the simplest and most economical method of obtaining continuous measurements of ionospheric effects. Much has been learned about the electron density distribution which exists along the path of the wave from these radio sounding experiments.

Breit and Tuve (1926) were the first to employ pulse transmissions to separate ionospheric echoes from the direct wave. By transmitting a short radio pulse and by measuring the time delay between the echo and the direct wave, the apparent reflection height (sometimes called group or virtual height) was deduced. The virtual height is defined as that height to which the pulse would travel in the measured time delay if it travelled at all times with the velocity of light. Since the electron density in the ionosphere at the height level from which the pulse is reflected is a known function of frequency, much can be learned from measurements of the variation of the apparent reflection height with frequency of the probing signal.

The ionosphere can be divided into two main regions - the E and F regions. The E-layer has its maximum electron density at a height of about 110 km and the F-region at a height of about 300 km. These values are only representative since diurnal and seasonal variations can often be quite complex. Often, during daylight hours, the F-region exhibits

a "bump" or a maximum of electron density below the main peak of the layer. When this occurs the lower of the two maxima is called the F_1 -layer and the upper is called the F_2 -layer. Further, during the daytime, there may be observed a region which has its maximum around 80 km and is known as the D-layer.

This study is only concerned with the lower ionosphere, e.g., the D and E-layers. From an experimental view point, the structure of the lower ionosphere (structure here referring to the electron density-height profiles) has been determined by ground based radio techniques and, in recent years, by means of rocket-borne experiments.

1.2 Previous Related Studies

Gardner and Pawsey (1953) measured the group heights and reflection coefficients of both magneto-ionic components of a 2 mc/s pulse transmitted with linear polarization. The electron density-height (N-h) profiles for the D-region were deduced from the slope of integrated differential absorption curves versus height for the two components.

Fejer (1955) obtained results from a pulsed wave interaction experiment on two frequencies near 2 mc/s. These N-h profiles agreed with those of Gardner and Pawsey, within an order of magnitude. Again, this technique is useful for D-region studies.

Many investigations by other ionospheric workers, including those at the Ionosphere Research Laboratory, have been carried out, and have been summarized by Waynick (1957).

Seddon, Pickar and Jackson (1954), Berning (1950), and others have deduced N-h profiles to heights including and well above the E-region using rocket-borne instrumentation or related techniques. Sweep-frequency radio sounding techniques in which the sounding frequency is varied over some specific range have long been in use in high frequency (1 mc/s and above) ionospheric research and have been put to use in low frequency work by Watts and Brown (1952) of the National Bureau of Standards. Lower frequencies are required for determining the structure of the lower ionosphere to insure reflections from the E-region rather than the upper regions of the ionosphere. An experiment similar to that of the National Bureau of Standards was placed in operation at the Ionosphere Research Laboratory at the Pennsylvania State University by Sechrist (1958) to permit routine sweep frequency group height recordings (sometimes abbreviated h'f) in the range 100 - 1000 kc/s. It was found, however, that such measurements did not yield sufficient information at these low frequencies to easily determine the electron density profile; a more complete understanding of the lower ionosphere can be obtained if the polarization characteristics of the reflected waves are simultaneously measured as well.

Parkinson (1955) used a crossed pair of loop antennas at a fixed frequency of 150 kc/s to measure the complete polarization characteristics (tilt angle, axial ratio, and sense of rotation) of the returned echoes. In this technique, a polarimeter was used in which the phase of the signal in one loop is advanced by $\pi/4$ and that of the other loop retarded by the same amount. Then the circular magneto-ionic components, known as ordinary and extraordinary, which will be defined later, are formed by the vector sum and difference of the phase shifted loop signals.

Carlson (1960a) adapted Parkinson's fixed frequency method to sweep frequencies but measured only the sense of rotation of the received polarization ellipse. Carlson's polarimeter, which has been in operation at the Ionosphere Research Laboratory since the experiment was begun, was used to obtain the records which are presented in Chapter 5 of this study.

Carlson (1960b) and Brunnschweiler (1960) were able to explain certain types of low frequency phenomena observed on the records; but in their analysis, ray theory was used and, furthermore, the influence of electronic collisions which take place in the lower regions was neglected. In general, these assumptions cannot be made for low frequency observations as may frequently be done for the reduction of high frequency ionograms. However, they gave proper justification for these assumptions when used in their interpretations.

1.3 General Statement of the Problem

The low frequency sweep sounding equipment which is in operation at the Ionosphere Research Laboratory is the only such experiment in the world now operating on a routine basis. The data which have been collected over the years contains a wealth of information. However, the involved theory of ionospheric radio wave propagation at low frequencies has made it extremely difficult to interpret but a few of these data.

Because of the very steep electron density gradients which can occur in the lower ionosphere, a full wave solution must be used to properly explain many of the features observed; this is indeed an involved investigation. There are several situations, however, in which records with large group retardations do occur over the sweep frequency range. It is these cases which permit an analysis of such records by an application of the more simplified ray theory.

1.4 Specific Statement of the Problem

For high frequency h'f data, ray theory has been successfully used to convert such data directly into electron density profiles. This theory is valid only if collisions are negligible, as they are at the higher frequencies. Somewhat similar methods of data reduction might be possible if the influence of collisions at the lower frequencies could be properly accessed. Upon this basis,

the specific aims of this investigation are:

- (1) To systematically investigate the effect of collisions upon group height computations for several realistic ionospheric models at D and E-region height levels over the sweep frequency range of 100 - 1000 kc/s.
- (2) To evaluate the results in order to determine the magnitude of the errors produced when collisions are neglected and to define what limitations must be placed upon frequency and model shapes, if any, in order that the simplified ray theory may be applied.

Although several workers have made group height computations with collisions included at certain selected frequencies, information pertaining to the degree in which they affect the propagation of radio waves, as far as group height is concerned, is still lacking. The objectives of this study, it is believed, will assist in the interpretation of low-frequency sweep records and extend the present knowledge of the electron density of the E-region.

2. MATHEMATICS OF GROUP HEIGHT

2.1 Full-wave Theory

Försterling (1942) showed that the vertical propagation of waves in a medium in which N and v are functions of height only is described by the coupled wave equations:

$$F''_O + F_O(k^2 n_O^2 + \psi^2) = \psi' F_X + 2\psi F'_X \quad (2.1)$$

$$F''_X + F_X(k^2 n_X^2 + \psi^2) = \psi' F_O + 2\psi F'_O \quad (2.2)$$

where

| | |
|---|--|
| $F_O = E_X^O(\rho_O^2 - 1)^{\frac{1}{2}}$ | describes the ordinary mode, |
| $F_X = E_Y^X(\rho_O^2 - 1)^{\frac{1}{2}}$ | describes the extraordinary mode, |
| $\psi = \rho_O' / (\rho_O^2 - 1)$ | is the coupling parameter, |
| ρ_O | is the wave polarization of the ordinary mode, |
| n_O, n_X | are the complex refractive indices. |

Let us consider the properties of such coupled equations. According to Budden (1961) the term "coupled equations" is usually given to a set of simultaneous, ordinary, differential equations with the following properties:

- (1) There is one independent variable.
- (2) The number of equations is the same as the number of dependent variables.
- (3) In each equation one dependent variable appears in derivatives up to a higher order than any other. The terms in this variable are called "principal" terms and the remaining terms are

called "coupling" terms.

- (4) The principal terms contain a different dependent variable in each equation, so that each dependent variable appears in the principal terms of only one equation.

It is often possible to choose the dependent variables so that the coupling terms are small over some range of height, as in the case for the Försterling equations; then the equations may be solved by successive approximations. As a first approximation the coupling terms are neglected and the resulting homogeneous equations, containing only the principal terms, are solved. These solutions are inserted in the coupling terms and the equations are again solved by the variation of parameters technique to give a better approximation. This method is obviously impracticable when any of the coupling terms become large.

The coupled equations for the most general case of oblique incidence would be very complicated for numerical computation; but Försterling's second-order equations for vertical incidence, which may be derived directly from Maxwell's equations and the constitutive relationships of the ionosphere, are much simpler than the oblique case so that they can be used for numerical computations.

Coupling is important at vertical incidence in two ways. There can exist a level in the ionosphere for which ψ is large, either because $X \approx 1$, the so-called coupling region, or the electron density gradient is large. When

this coupling is strong it can give rise to the Z-trace at the higher frequencies and to the " coupling echo" at lower frequencies. At low frequencies even though Ψ can be small it can have a cumulative effect over a large range of height. It has been shown from first order solutions to the Försterling equations that an up-going ordinary wave gives rise to a down-going extraordinary wave from the coupling region, and vice versa. There is then the possibility that there will be a direct echo from the coupling region. The presence of a coupling echo can indicate that the ionosphere is not slowly varying. This is most likely to occur when the wave length is long and explains why coupling echoes are not usually seen above 500 kc/s.

Much progress has been made in developing approximate solutions of these coupled wave equations, and the reader is referred to the works of Gibbons and Nertney (1952), Davids (1955), Budden (1955), Johler (1962), and Ferraro and Gibbons (1958).

2.2 Ray Theory

If N is slowly varying, then Ψ can be shown to be small and the equations (2.1) and (2.2) reduce to

$$F''_O + k^2 n_O^2 F_O = 0 \quad (2.3)$$

$$F''_X + k^2 n_X^2 F_X = 0 \quad (2.4)$$

which shows that the ordinary and extraordinary waves propagate independently. These equations cannot be solved

in closed form, except for a few specialized functional forms for n_0 and n_x , but if the complex refractive index is slowly varying one can apply the approximate W.K.B. solution

$$F = n^{-1/2} \exp \left[-jk \int_0^x n dh \right] \quad (2.5)$$

This expression is quite accurate provided

$$\frac{1}{k^2} \left| \frac{3}{4} \left(\frac{1}{n} \frac{dn}{dh} \right)^2 - \frac{1}{2} \frac{1}{n^3} \frac{d^2 n}{dh^2} \right| \ll 1 \quad (2.6)$$

This condition is best met at high frequencies on account of the factor $1/k^2$, but no matter how high the frequency or how small the derivatives, the condition is sure to fail at a level where n passes through a zero. At this point we have a reflection condition for the wave and the W.K.B. solution breaks down. For a more detailed theory of the properties of the W.K.B. solution it is suggested that the reader refer to Budden (1961).

It is seen from the form of the solution given by (2.5) that the ray suffers an absorption and phase shift, in that n can be complex, as the ray propagates through the ionospheric medium.

Although ray theory involves many approximations, its use is permissible in explaining several features of ionospheric propagation, particularly at high frequencies. At lower frequencies the ionosphere can change appreciably within a distance of one wave length, and cannot always be regarded as a slowly varying medium. Then the W.K.B.

solution may fail to be a good approximation, and a full wave-solution is required.

Whenever the coupling parameter is large, as will be the case when the derivative of the polarization term is approximately equal to one, ray theory can no longer be used and this can occur at the level where $N = N_c$.

Thus far only continuous wave solutions have been described; let us now consider a pulsed wave. Following an analysis similar to Gibbons and Rao (1957), but correcting an error which appeared in their paper, the transmitted pulse may be considered to have a Gaussian envelope and thus represented by

$$f(t) = Ae^{-(t/T)^2} e^{j\omega_0 t} \quad (2.7)$$

where ω_0 is the carrier frequency of the pulse, T the time for the envelope to drop to $1/e$ of its maximum value A . The Fourier transform of $f(t)$ is also a Gaussian spectrum of the form

$$\frac{AT}{\sqrt{2}} e^{-\frac{T^2}{4} (\omega - \omega_0)^2} \quad (2.8)$$

and thus $f(t)$ may be considered to be the superposition of an infinite number of carrier waves,

$$f(t) = \frac{AT}{\sqrt{2}} \int_{-\infty}^{+\infty} e^{-\frac{T^2}{4} (\omega - \omega_0)^2} e^{j\omega t} d\omega \quad (2.9)$$

We may now consider that each carrier wave of frequency ω has a complex reflection coefficient $R(\omega)e^{-j\theta(\omega)}$ which would specify the amplitude and phase of that particular

wave at the receiving station after ionospheric reflection.

The pulse received after reflection would then be

$$F(t) = \frac{AT}{2\sqrt{\pi}} \int_{-\infty}^{+\infty} R(\omega) e^{-j\phi(\omega)} e^{-\frac{T^2(\omega-\omega_0)^2}{4}} + j\omega t \, d\omega. \quad (2.10)$$

We now assume that $R(\omega)$ and $\phi(\omega)$ across the band of frequencies contributing significantly to the pulse have the linear form

$$R(\omega) = R_0 [1 + p(\omega - \omega_0)] \quad (2.11)$$

$$\text{and} \quad \phi(\omega) = \phi_0 + q(\omega - \omega_0). \quad (2.12)$$

The above can be considered to be the first two terms of a Taylor series expansion. Making the substitution

$W = \omega - \omega_0$, the expression for the received pulse then appears as

$$F(t) = \frac{e^{-j\phi_0}}{2\pi} ATR_0 e^{j\omega_0 t} \int_{-\infty}^{+\infty} (1+pW) e^{-\left(\frac{TW}{2}\right)^2 + jW(t-q)} \, dW. \quad (2.13)$$

This integrates to

$$F(t) = e^{-j\phi_0} ATR_0 e^{j\omega_0 t} \left[1 + \frac{2jp(t-q)}{T^2} \right] e^{-\left(\frac{t-q}{T}\right)^2}. \quad (2.14)$$

If p , the rate of change of received amplitude with frequency, was zero the received pulse would have the same shape as the transmitted pulse, but the maximum would be delayed by a time q . If the phase index of the ionospheric medium at ω_0 is $\mu(h, \omega_0)$, the total phase path would be $2\int \mu dh$ by ray theory; that is, the distance which would be traveled in the same time, if the phase velocity of the

wave was everywhere c , the velocity of light in vacuum. The time delay $q = d\theta/d\omega$ can be obtained in the following way. The phase delay $\theta(\omega)$ can be found by taking

$$2 \int_0^{h_r} \mu(\omega) 2\pi/\lambda_0 dh. \quad \text{Then}$$

$$q = \frac{\partial \theta}{\partial \omega} = \frac{2}{c} \int \frac{\partial}{\partial \omega} (\mu \omega) dh = \frac{2}{c} \int \left(\mu + \omega \frac{\partial \mu}{\partial \omega} \right) dh, \quad (2.15)$$

so that setting $qc/2$ equal to the virtual reflection height h' , one finds that

$$h' = \int_0^{h_r} \left(\mu + \omega \frac{\partial \mu}{\partial \omega} \right) dh = \int_0^{h_r} \mu' dh \quad (2.16)$$

where $\mu + \omega \partial \mu / \partial \omega$ is designated by μ' which is called the group refractive index of the medium.

In the above formulation for the group height, ray theory was employed to find the phase, θ , by integrating μ up to the classical reflection point; i.e., the height at which μ becomes zero when collisions are absent. When collisions are present, μ can become quite small near the classical reflection point, but not zero. This raises some question as to how to employ the ray theory in this situation. Gibbons and Rao (1957) used some fairly exact wave solutions to find the phase at two closely spaced frequencies so that $\partial \theta / \partial \omega$ could be approximated by $\Delta \theta / \Delta \omega$. They found that computing the virtual heights in this manner at 150 kc/s for the extraordinary mode compared very favorably with the integral of μ' up to the classical reflection level. In fact μ' drops sharply above this level so that any uncertainty in the upper limit of integration has negligible effects.

Rydbeck (1942) investigated the validity of ray theory with collisions neglected for a parabolic layer whose semi-thickness was 120 km, and compared the exact virtual heights obtained by a full wave treatment to that using ray theory. He found that they differed only in a very narrow region near the peak of the layer, provided that the layer is not thick compared with a wave length.

Thus there is strong encouragement for the continued use of the ray theory when collisions are present. The next section describes another procedure for including collisions in group height computations through the use of the phase integral technique.

2.3 The Phase Integral Method

Budden (1961) has proposed that when collisions are considered, the phase path P is equal to the real part of the contour integral of the complex refractive index, n , from $X = 0$ (ground level) to the point in the complex plane at which n becomes zero. This is at $X = 1 - jZ$ for the ordinary mode. The virtual height will, according to Budden, be given by the integral equation

$$h' = \operatorname{Re} \int_0^{1-jZ} n' \frac{dh}{dX} dX = \int_0^1 \mu' \frac{dh}{dX} dX + \operatorname{Re} \int_1^{1-jZ} n' \frac{dh}{dX} dX \quad (2.17)$$

where $n' = n + f \frac{\partial n}{\partial f}$ and $\mu' = \operatorname{Re}(n')$. The virtual heights obtained by the ray theory method of integrating μ' up to $X = 1$ would be correct, according to the above equation if the last integral in (2.17) was small. This will be the

case when the collision frequency is small and when dh/dX is small.

In this formulation the collision frequency, ν , must be assumed constant; this condition is, of course, unrealistic. This would be a valid assumption if the base of the ionosphere started in a region in which the electron collisions were small. It will be shown in Chapter 3 that, for values of ν between zero and one-thousand, the group refractive index, μ' , will only be affected at and very near the reflection points. However, in the lower ionosphere, the collisions are much more frequent and have a more pronounced affect on the group refractive index.

Budden gives two further conditions which are necessary for the phase integral formula to be valid. These are the following:

(1) The square of the refractive index, n^2 , must vary linearly with height over a range near the reflection level where $n = 0$.

(2) There must be a range of height where the W.K.B. solutions are good approximations, that is where (2.6) holds, and this must extend from the ground into the region where (1) applies.

Since the left side of (2.6) is inversely proportional to the square of the frequency, this condition is most easily violated at low frequencies.

Because of the restrictions placed upon the use of the phase integral technique, particularly constant collisions

and linear variation of n^2 near the reflection level, all group height computation to be presented and discussed in this work will be based upon the use of equation (2.16). As mentioned earlier, the excellent agreement between this method and the full-wave theory of Gibbons and Rao gives encouragement for the use of the ray theory approach.

2.4 The Conversion of h'f Records to N-h Profiles

Approximate methods for obtaining N-h profiles from h'f records have been known for several years. Until the advent of high speed digital computers these processes have been considered too laborious for reducing any great number of records without first making simplifying approximations.

The apparent height of reflection is given by

$$h'f = \int_0^{h_r} u'(f, N) dh = \int_0^f u' \frac{dh}{df_n} df_n \quad (2.18)$$

where u' is the group refractive index, f is the operating frequency, h_r is the height of reflection, h is the height above the ground, $N(h)$ is the electron density at height h , and f_n is the plasma frequency.

The problem of deducing the N-h profile now consists of finding a function $N(h)$ which satisfies (2.18). The solution of (2.18) can be approached by two methods:

- (1) Model methods: The shape of the profile is assumed and substituted into (2.18), which gives an integral which can be evaluated analytically. The calculated h'f curve is then compared with

the one observed, and the parameters are varied until the best match with the actual record is found.

- (2) Integral equation methods: The integral equation method can be divided into two classes. In the first, the equation is inverted directly and solved analytically. In the second, the integral is replaced by a discrete sum over a number of plasma frequency intervals. The first is known as the direct integral method and the latter, the lamination method. The lamination method represents a most important advance in this field.

Thomas (1959) has given an excellent review and a complete bibliography of the more usual methods of obtaining N-h profiles from h'f curves. Schmerling (1957) has programmed the Budden matrix inversion method and has discussed the limitations of this method, as well as other methods.

One difficulty is due to the "valley ambiguity". When the F1 layer is present, there may exist a decrease in the electron density above this layer. Since the integral equation method assumes a monotonic distribution with height, e.g., dh/df_n of (2.18) is single valued, this condition will give results which are not strictly valid. This method, if applied to an h'f curve which was produced from a profile with a valley, in general, will not give the actual profile, but an "equivalent" profile. The

monotonic "equivalent" profile, which would give rise to the observed h'f curve, is everywhere lower than the actual profile above the F1 peak. The effect of filling in the valley is to over-correct for group retardation.

The other main difficulty of the integral equation method is due to the "low frequency cut-off". Some assumption must be made in all inversions of the integral equation method concerning the missing portion of the observed h'f curve below the cut-off frequency. The usual assumption made is that the curve can be extrapolated down to zero frequency at a constant height at which the cut-off frequency is reflected. Often, when observing echoes from the E-region, the h'f curves will be very flat; therefore, the above assumption appears to be reasonable. However, this assumption may produce considerable errors near sunrise and other times when there is underlying ionization which is not observed.

In all the methods mentioned, the effect of electron collisions has been neglected, but most include the earth's magnetic field. These methods of inversion can be applied to low frequency sweep ionograms, provided the limitations of zero collision models are understood at these low frequencies; this, indeed, is the objective of this study.

3. THE GROUP INDEX OF REFRACTION INCLUDING COLLISIONS AND MAGNETIC FIELD

3.1 Appleton-Hartree and Mu Prime Equations

Following the notation used by Budden (1961), the complex refractive index of an ionized medium which has a superimposed steady magnetic field, and in which electronic collisions take place, is given by

$$n^2 = 1 - \frac{X}{1 - jZ - \frac{1}{2}Y_T^2 / (1 - X - jZ) \pm \left[\frac{1}{4}Y_T^4 / (1 - X - jZ)^2 + Y_L^2 \right]^{1/2}} \quad (3.1)$$

This is the Appleton-Hartree equation which, as a first approximation, governs much of the theory of radio wave propagation.

In the case when collisions are neglected ($Z = 0$), the Appleton-Hartree equation reduces to

$$n^2 = 1 - \frac{X}{1 - \frac{1}{2}Y_T^2 / (1 - X) \pm \left[\frac{1}{4}Y_T^4 / (1 - X)^2 + Y_L^2 \right]^{1/2}} \quad (3.2)$$

The three zeros of n^2 , which correspond to reflection conditions, occur when $X = 1$ and $X = 1 \pm Y$.

The Appleton-Hartree equation simplifies to

$$n^2 = 1 - X \quad (3.3)$$

for the case of no imposed magnetic field and no collisions. Here the only reflection condition occurs when $X = 1$.

For a more detailed discussion on these and other

special properties of n^2 the reader is referred to Ratcliffe (1958).

As stated in Chapter 2, the group refractive index, μ' is given by $\mu' = \mu + f \frac{\partial \mu}{\partial f}$. When Z is not zero, i.e., when the effect of collisions is included, the value of n^2 is complex. By writing μ' as the real part of $n' = \text{Re}(n + f \frac{\partial n}{\partial f})$, it can be shown by direct differentiation of (3.1) that

$$\begin{aligned} \mu n' - 1 = \frac{1}{D} \left(-X + \frac{1}{2} j X Z + (1 - n^2) \left[1 - j Z - \frac{1}{2} j X Z \right. \right. \\ \left. \left. + \frac{1}{2} (1 - X - j Z)(1 + X) Y_L^2 \left[Y_L^2 (1 - X - j Z)^2 + \frac{1}{4} Y_T^4 \right]^{-\frac{1}{2}} \right] \right) \end{aligned} \quad (3.4)$$

where

$$D = (1 - j Z)(1 - X - j Z) - \frac{1}{2} Y_T^2 \pm \left[Y_L^2 (1 - X - j Z)^2 + \frac{1}{4} Y_T^4 \right]^{\frac{1}{2}} \quad (3.5)$$

Thus, by computing n directly from (3.1) and utilizing the above result, the group refractive index, μ' , is determined. The detailed steps involved in employing (3.4) are summarized in Appendix A.

Several methods for obtaining values of μ' have been developed by other workers. Gibbons and Rao (1957) used accurately tabulated values of the Appleton-Hartree equation to find μ , and plotted graphs of μ against frequency for various values of N and ν . Then $\frac{\partial \mu}{\partial f}$ was obtained by placing a tangent to this graph at the required operating frequency. This method was found to be sufficiently accurate for low values of electron density for which the curves were slowly varying with frequency; however, the method failed to give accurate results for high values of electron density,

particularly near the reflection points, because of the sharp changes in μ . Abandoning this method, they computed values of μ at two closely spaced frequencies using an approximate form of the Appleton-Hartree equation. This procedure yielded excellent results for the extraordinary mode at and near the reflection point $X = 1 + Y$, but was very unreliable near the $X = 1$ level because of the approximate form of the Appleton-Hartree equation. As will be shown in this chapter, it is near this level that profound changes in μ' can occur because of collisions. As a result, workers who have used these approximate μ' values may find their computations seriously in error.

A more general method is to utilize the exact form of (3.4). This is a very complicated and tedious method; but, with the aid of a high speed digital computer, the problem is feasible, and allows one to exercise great flexibility in choosing the ionospheric parameters.

Such a computer program was developed and was used to obtain the values of μ' presented later in this chapter. The Appleton-Hartree equation has been previously solved for μ and x by Mechtly (1959). A similar approach was used here, but in a different coordinate system and in the MKS unit system. Mechtly's program was adapted for use on PENNSTAC, the digital computer in the Electrical Engineering Department. His program gives only μ , x , the polarization terms, and an accuracy check for one set of parameters in eighty seconds. This program was extended for use on the IBM 7074, which gives all the above data, in addition to μ' ,

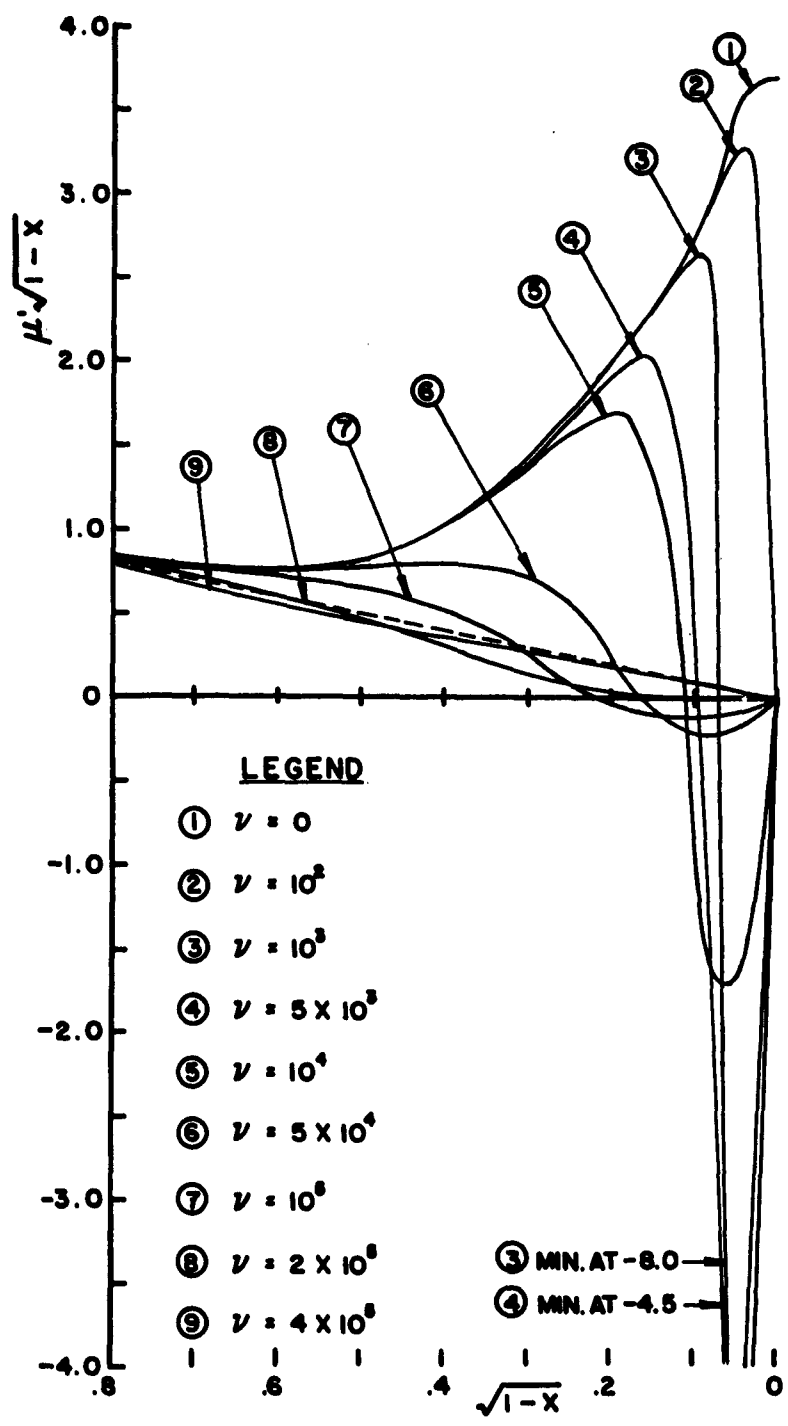
in 0.4 second.

It is well at this stage to define what is meant by the extraordinary and ordinary modes. Using the convention followed by Budden, ordinary will be termed that mode for which μ' tends to infinity as X approaches unity with collisions set to zero. The other mode, extraordinary, will have a singularity in μ' at that level where $X = 1 + Y$.

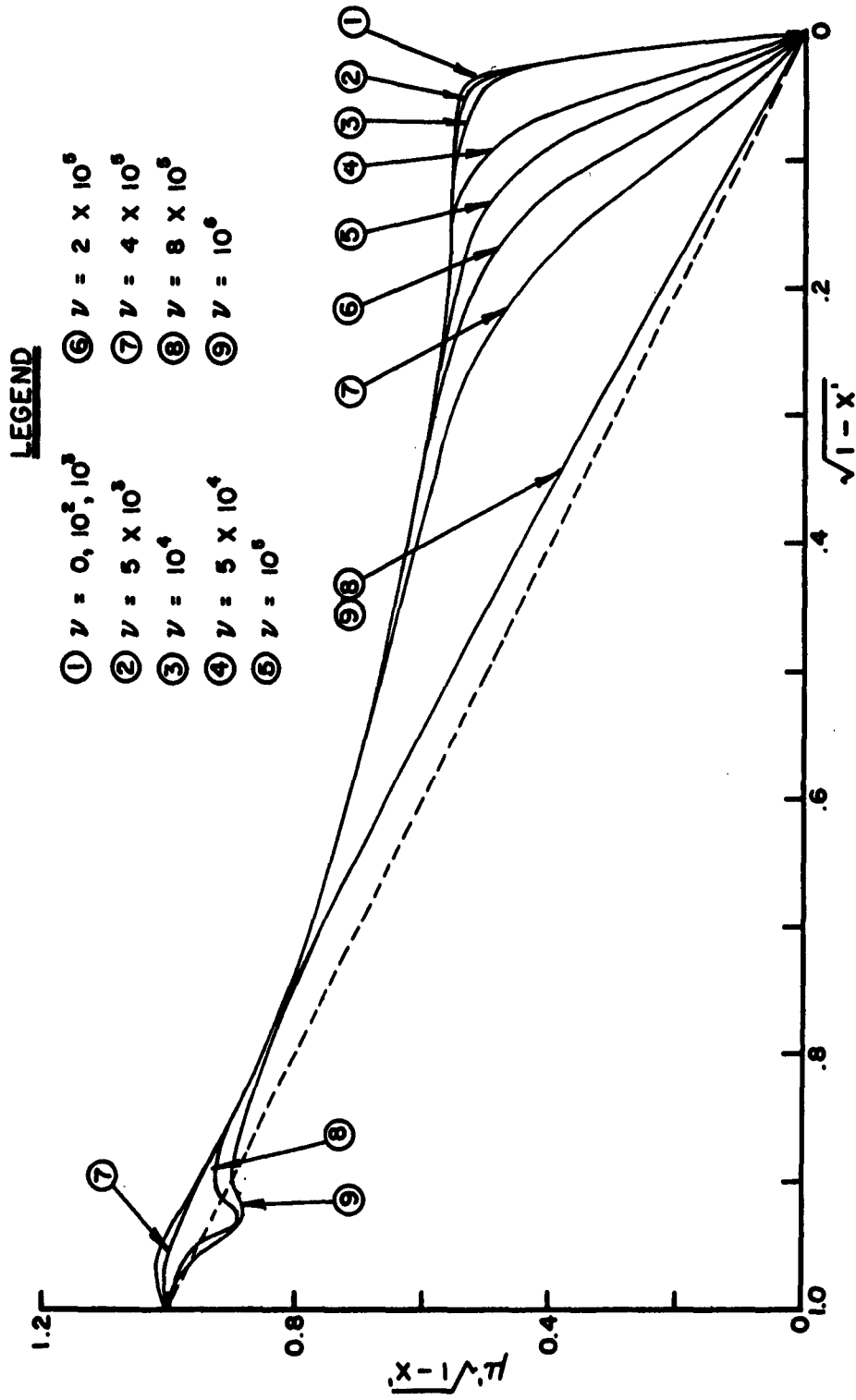
As to which sign in front of the square root of (3.5) should be used to correspond to these modes depends upon the ionospheric profile utilized. Since it is possible for a discontinuity in the index to occur at $X = 1$, the reader is referred to Appendix A for a discussion as to what sign should be used to maintain continuity.

3.2 Presentation of the μ' Curves

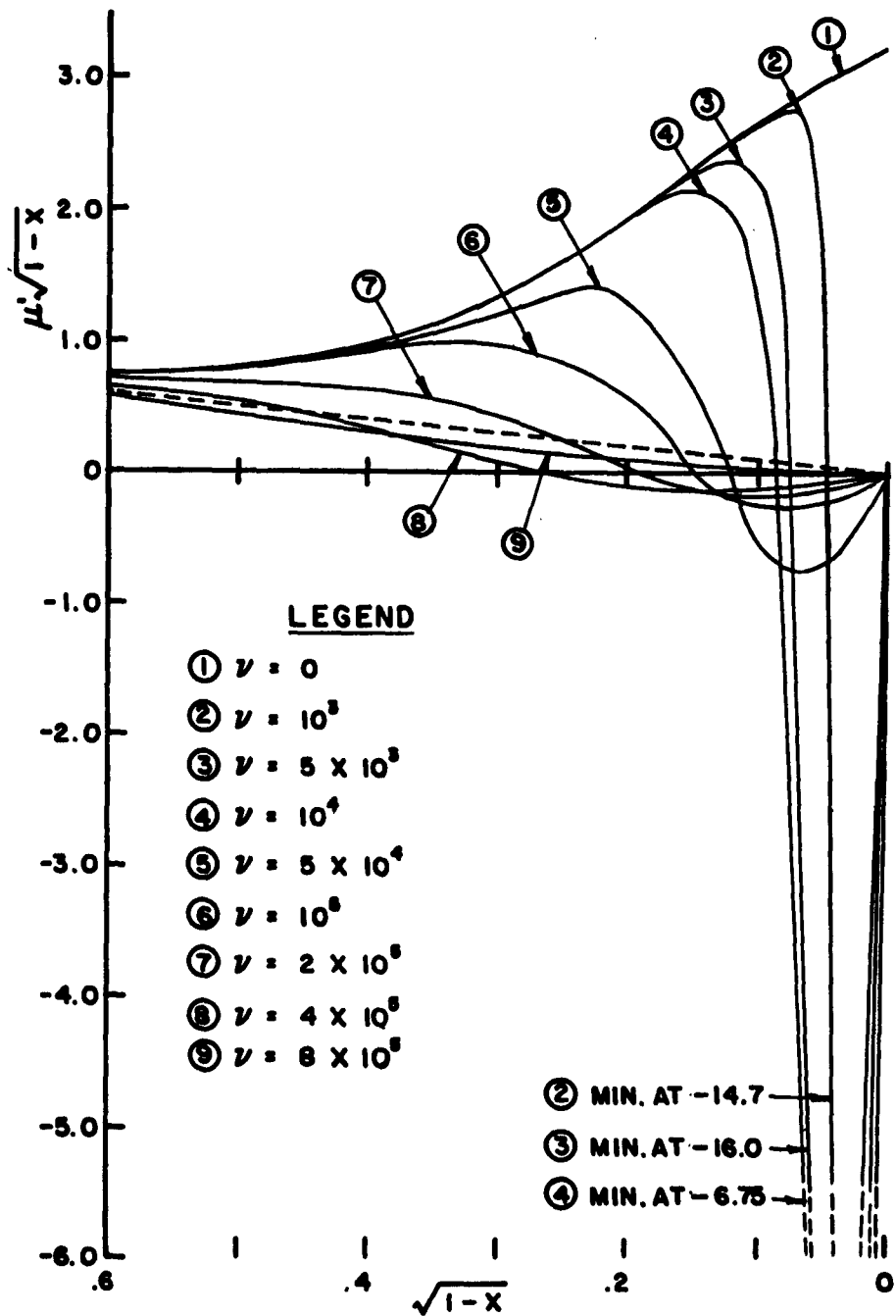
Titheridge (1961) has shown curves noting the effect of collisions on the propagation of radio waves in the ionosphere. In his paper the majority of the frequencies used were those above the gyro-frequency. It is the aim of this section to show similar curves for frequencies below the gyro-frequency, i.e., in the sweep frequency range 100 - 1000 kc/s used at the Ionosphere Research Laboratory for sounding experiments. These curves show the variation of μ' for a constant collision frequency with increasing values of electron density. For the ordinary mode, curves of $\mu'\sqrt{1 - X}$ are plotted against $\sqrt{1 - X}$, so that the function plotted is always finite and the region near $X = 1$ is expanded. In a



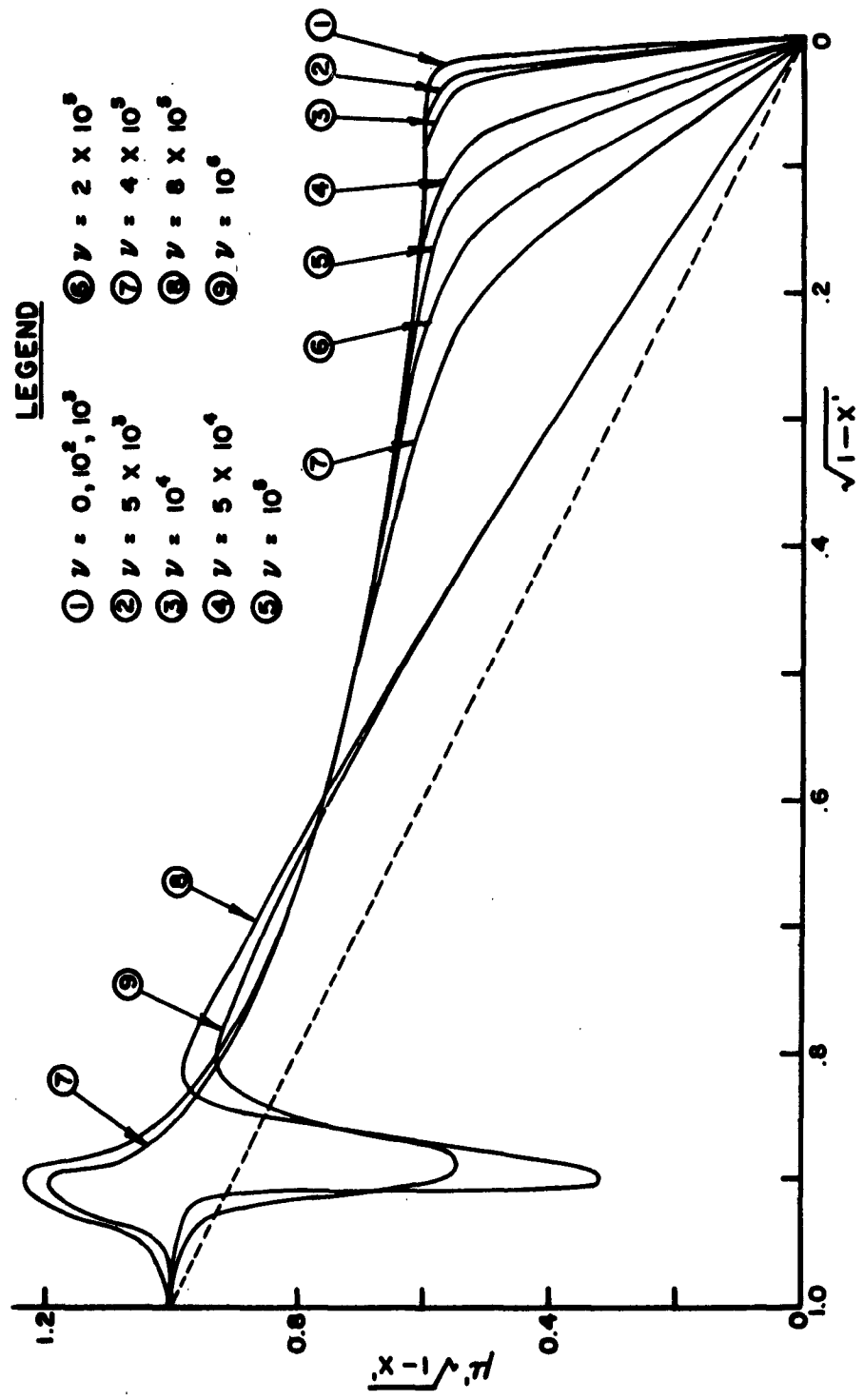
THE GROUP REFRACTIVE INDEX FOR THE ORDINARY RAY AT 100 KC
FIGURE 1



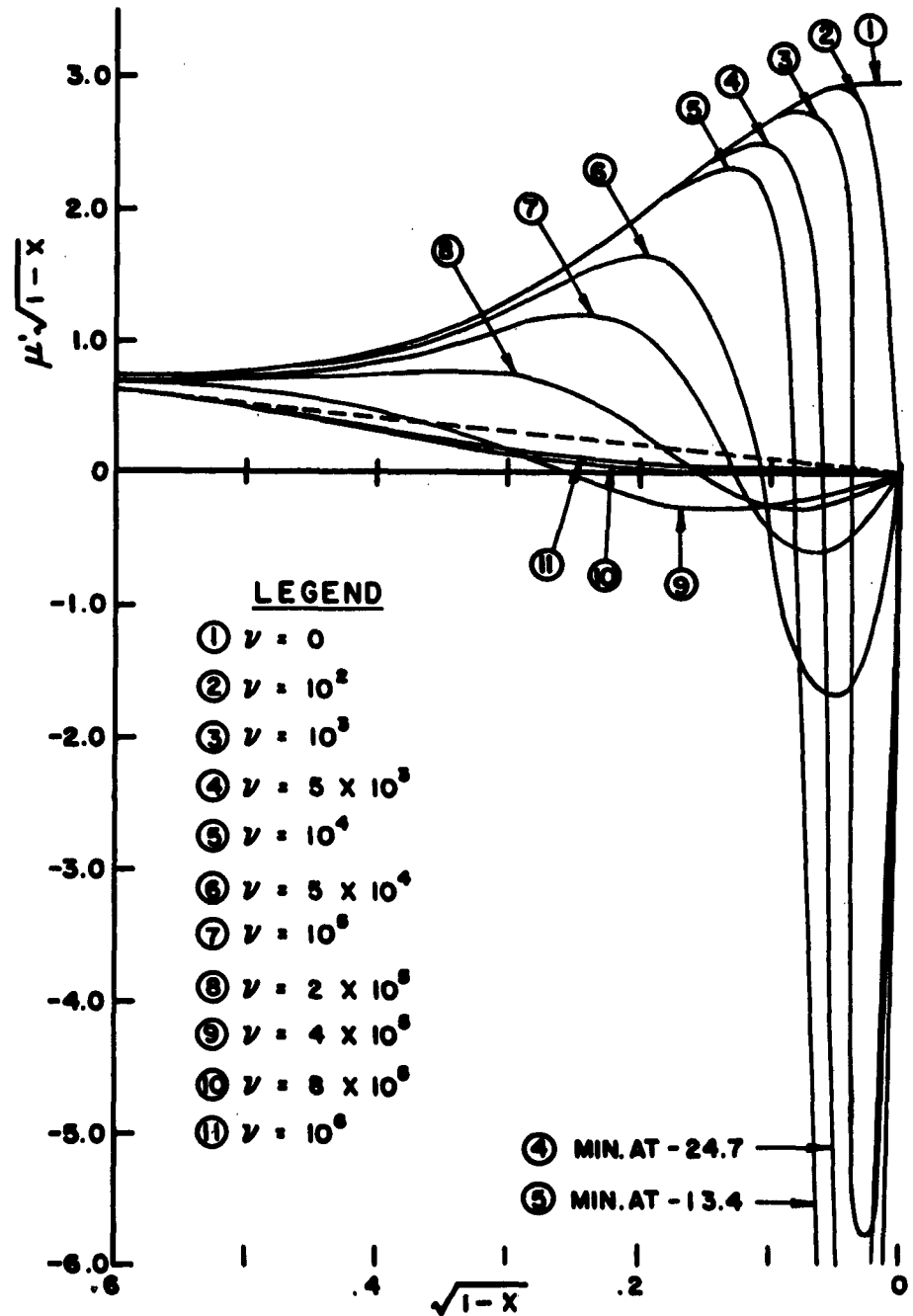
THE GROUP REFRACTIVE INDEX FOR THE EXTRAORDINARY RAY AT 100KC
FIGURE 2



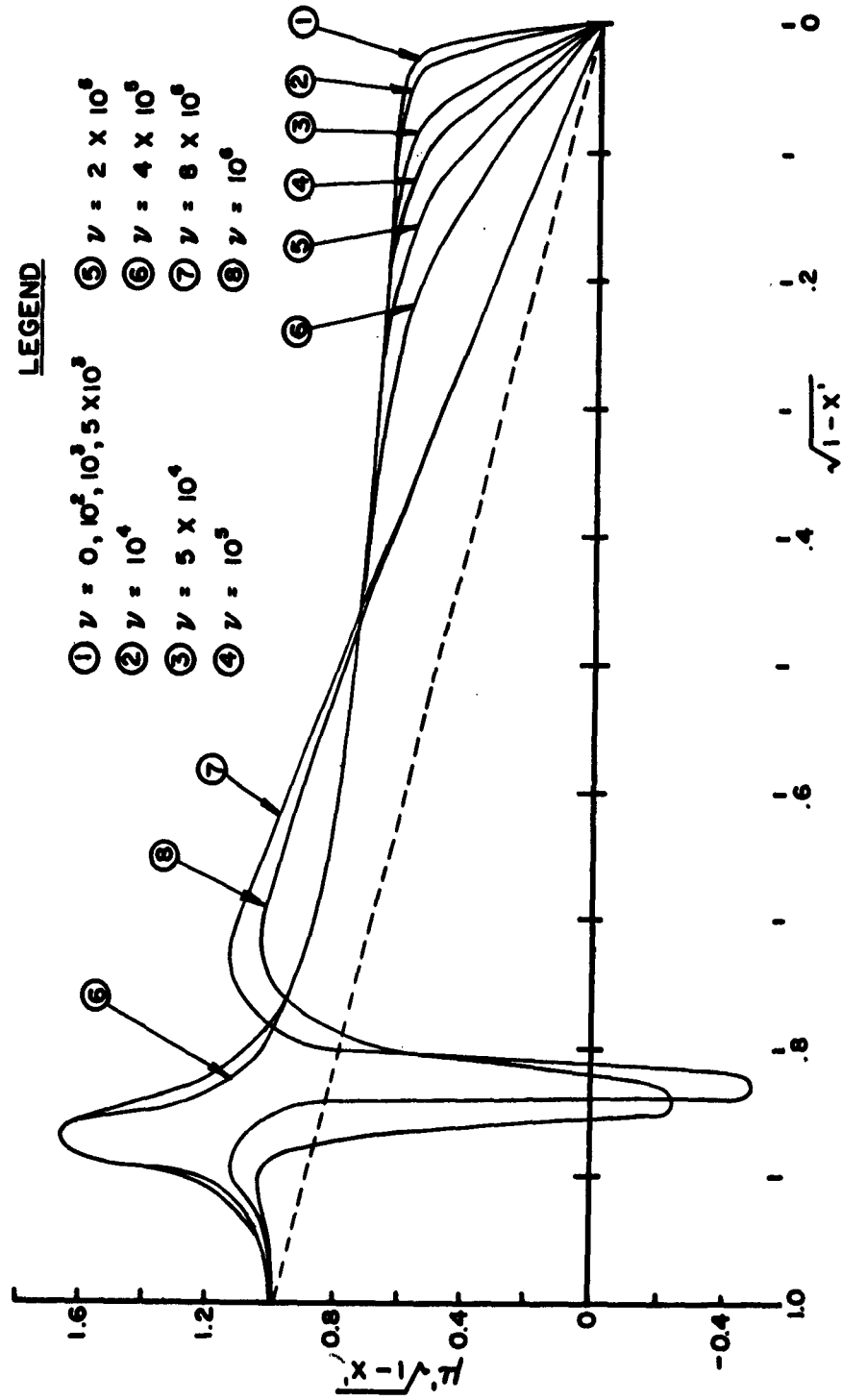
THE GROUP REFRACTIVE INDEX FOR THE ORDINARY RAY AT 300 KC
 FIGURE 3



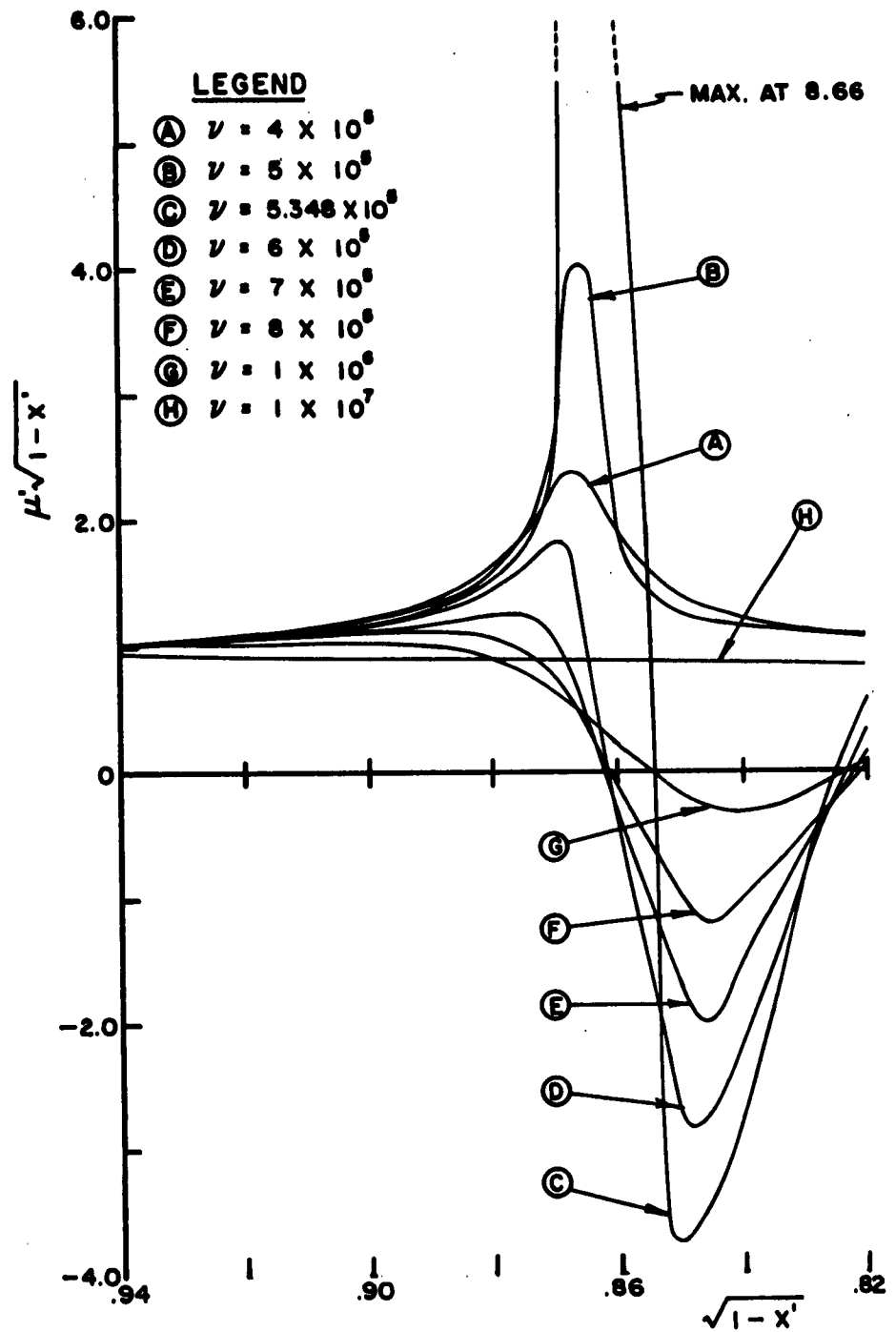
THE GROUP REFRACTIVE INDEX FOR THE EXTRAORDINARY RAY AT 300 KC
FIGURE 4



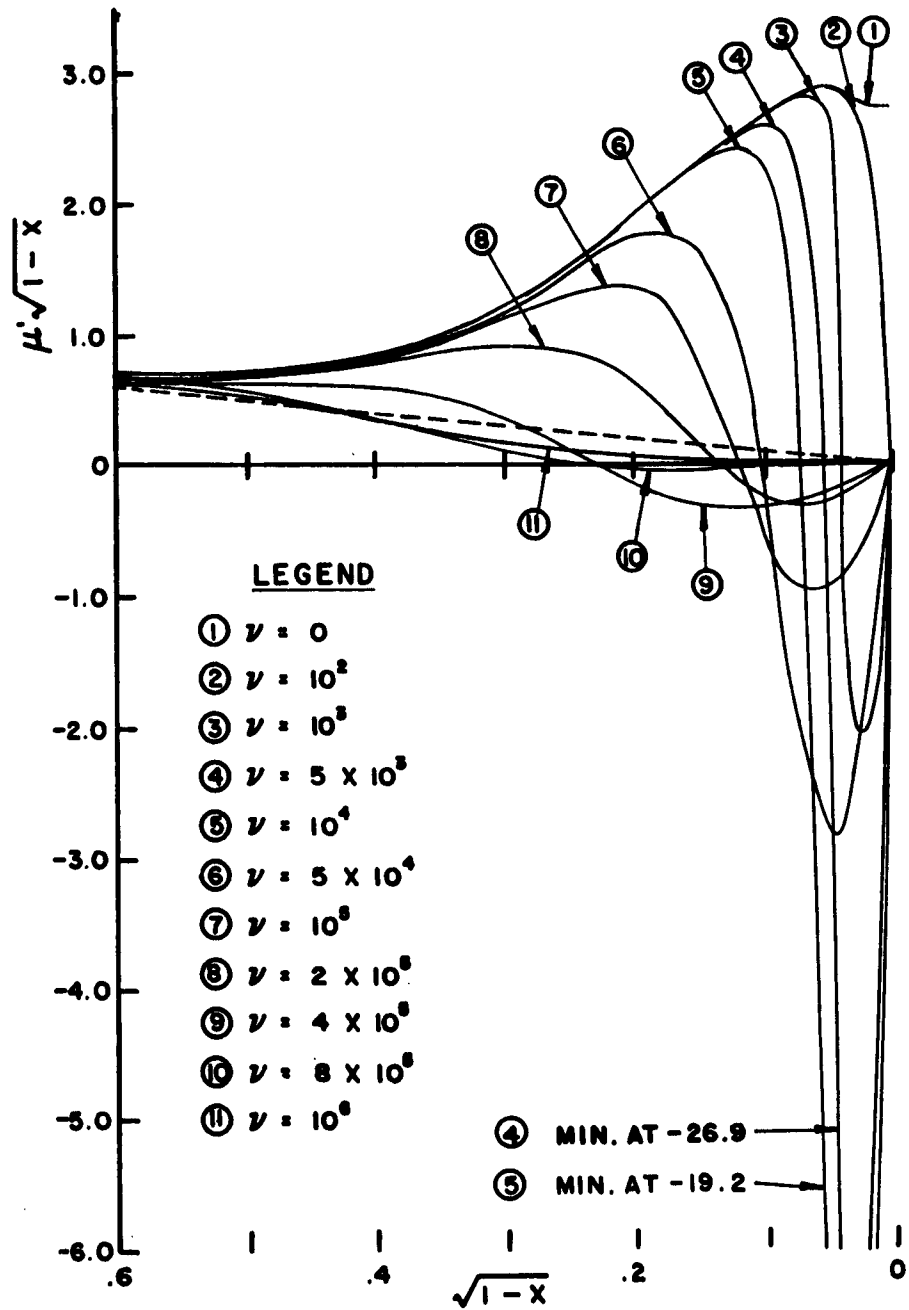
THE GROUP REFRACTIVE INDEX FOR THE ORDINARY RAY AT 500KC
FIGURE 5



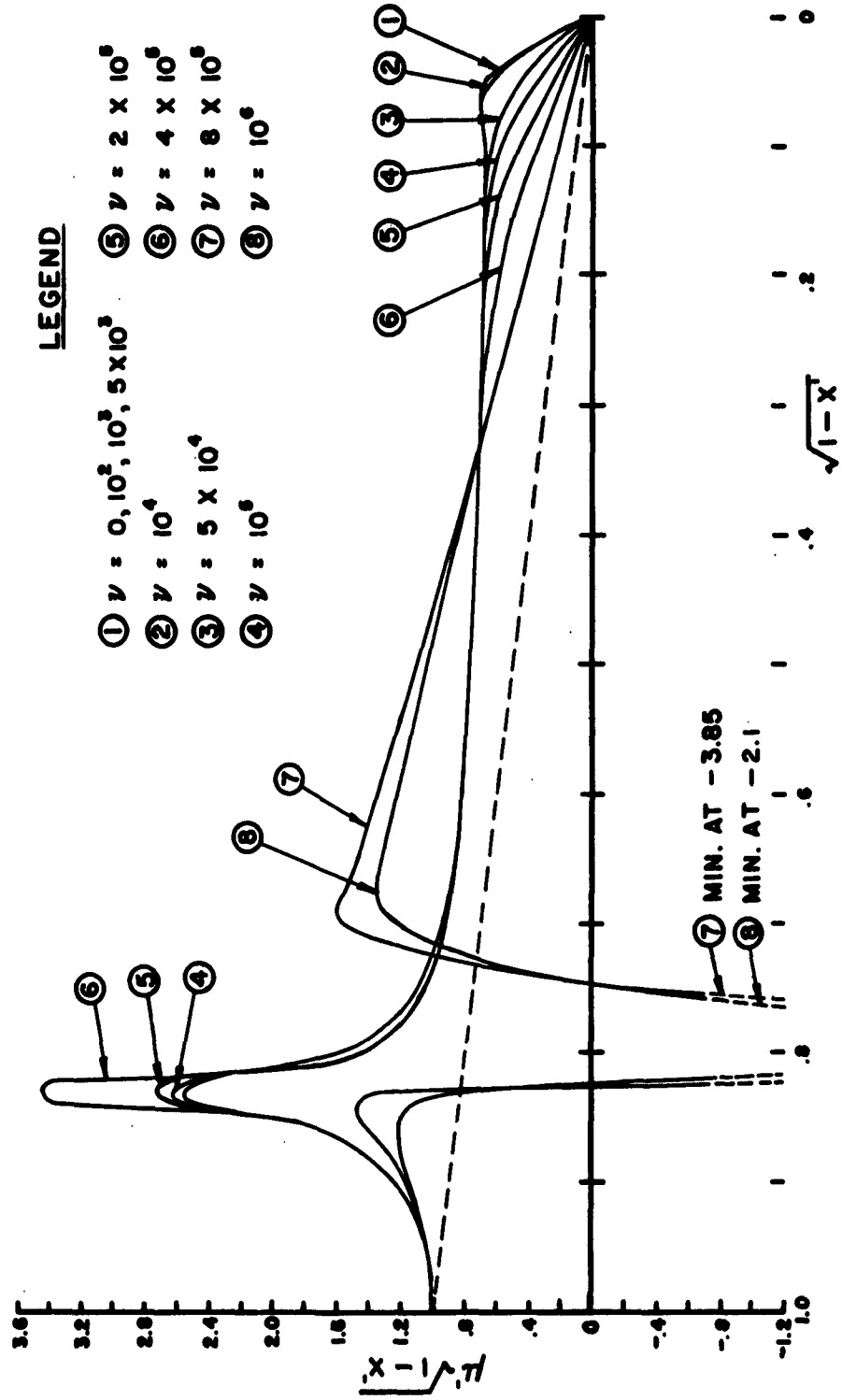
THE GROUP REFRACTIVE INDEX FOR THE EXTRAORDINARY RAY AT 500 KC
FIGURE 6



EXPANDED VIEW OF FIGURE 6 AROUND $x = 1$ AND $1/2$
FIGURE 7

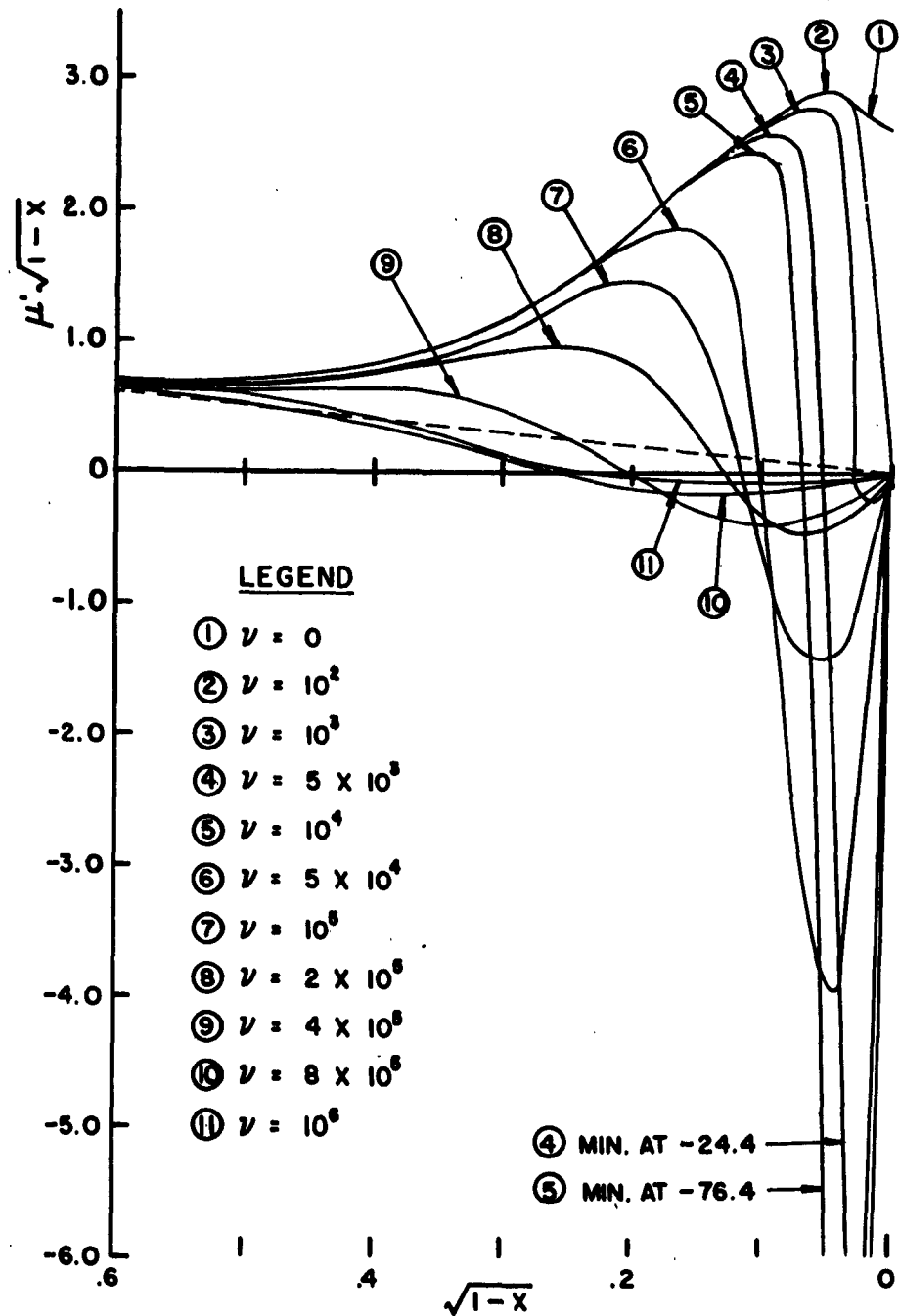


THE GROUP REFRACTIVE INDEX FOR THE ORDINARY RAY AT 700 KC
FIGURE 8

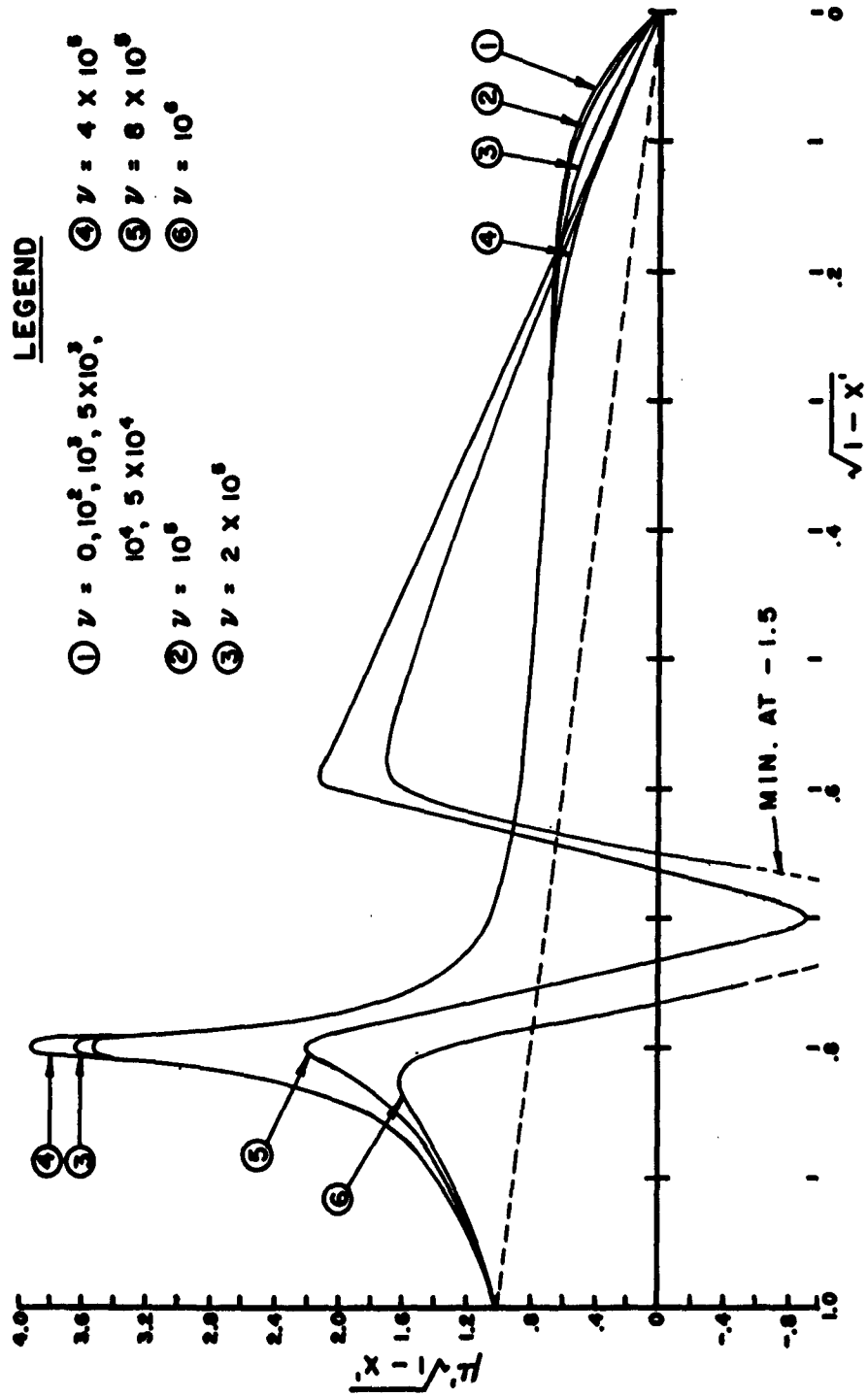


THE GROUP REFRACTIVE INDEX FOR THE EXTRAORDINARY RAY AT 700 KC

FIGURE 9



THE GROUP REFRACTIVE INDEX FOR THE ORDINARY RAY AT 900 KC.
FIGURE 10



THE GROUP REFRACTIVE INDEX FOR THE EXTRAORDINARY RAY AT 900 KC
FIGURE 11

similar manner, for the extraordinary, $\mu' \sqrt{1 - X'}$ is plotted against $\sqrt{1 - X'}$ where $X' = X/(1 + Y)$, so that the extraordinary is reflected where $X' = 1$. In all cases considered Y was larger than unity. The straight line plotted on these curves corresponds to $\mu' = 1$; any curves which drop below this line will have a $\mu' < 1$.

Families of curves were made for ten frequencies covering the range 100 - 1000 kc/s in steps of 100 kc/s; however, to conserve space, only the odd frequencies are presented (see Figures 1 - 11). Figure 7 is an expanded view of Figure 6 around the point $X = 1$ and the critical collision frequency. Other curves similar to this, and with similar results were obtained, but will not be presented in this work. One of these should serve to illustrate the rapid changes which occur in this region due to the presence of collisions.

3.3 General Discussion of the Influence of Collisions

The ordinary mode curves will be discussed first. The general appearance of all the ordinary mode curves is much the same and the following characteristics are noted.

The most striking feature of these curves is the negative values of μ' ; μ' less than unity implies a group velocity greater than the velocity of light. Since this cannot occur, one can only conclude that the ray theory is not valid for these cases. The $X = 1$ level is that region where coupling can be important; as discussed in Chapter 2, full-wave solutions are required. Thus for the ordinary mode, it must be concluded that ray theory with collisions

is not applicable to the reduction of low frequency ionograms. This is not the case with the extraordinary mode, as we shall see.

These negative values of μ' occur for collision frequencies of 10^3 -sec⁻¹, and larger, and are largest between 10^3 and 10^4 -sec⁻¹. For frequencies 500 kc/s and smaller, μ' remains positive for values of ν greater than 8×10^5 -sec⁻¹; however, the value of the phase refractive index, μ , is near unity which indicates very weak reflections that could not be detected.

It should be pointed out that when $\nu = 0$, the value of μ' tends to infinity as X approaches 1; however, due to the method of plotting these curves, $\mu' \cdot 1 - X$ tends to a finite limit as X approaches 1 for the zero collision case.

The general effect of collisions is to keep μ' from becoming infinite at $X = 1$; increasing the collisions reduces the positive hump of μ' near the reflection point. For values of $\nu = 8 \times 10^5$ -sec⁻¹ and larger, μ' approaches unity. This is true for all frequencies shown, but more so at the lower frequencies.

For X smaller than 0.65, which corresponds to $\sqrt{1 - X} = 0.6$, the values of μ' are approximately equal to each other for all values of ν and all frequencies. As the frequency increases, the values of μ' remain approximately equal over a larger range of X . As X approaches zero, μ' approaches unity.

All the extraordinary mode curves follow a definite

pattern in which the variations become more pronounced as the frequency is increased.

The most noticeable pattern is the positive hump and negative values which occur near the center of the curve. This hump corresponds to the point $X = 1$. This peak increases with increased collisions and has its largest value at the critical collision frequency ($\nu_c = 5.348 \times 10^5 \text{ sec}^{-1}$ for State College, Pennsylvania). For ν equal to and slightly larger than ν_c , the value of μ' becomes negative. As ν is increased above 10^7 sec^{-1} , μ' is approximately equal to unity. Figure 7, which is an expanded view of Figure 6 around the point $X = 1$ and ν_c , clearly illustrates these features. Figure 7 also indicates that both the largest positive and negative values for this region occur at ν_c . Again, as for the ordinary mode, ray theory is not valid for those specific values of ν which make μ' negative. The height range corresponding to the collision frequencies where μ' for $X = 1$ becomes negative is 65 to 86 km. These values were obtained from the collision frequency vs. height curve (Figure 12), used to determine the collision frequency as a function of height for the computations of virtual heights in Chapter 4.

To further display the influence of collisions on μ' at $X = 1$ and $X = 1 + Y$, values of μ' for three wave frequencies, 100, 500, and 1000 kc/s, and various collision frequencies are shown in Table 1. Referring to this Table it will be noted that the "bump" corresponding to the region

TABLE 1

Extraordinary Mode Mu Primes At Reflection Levels

| | μ' at N_c | | | μ' at N_y | | |
|---------------------------------------|-----------------|-------|-------|-----------------|-------|-------|
| $\nu - \text{sec}^{-1}$ Freq(kc/s) | 100 | 500 | 1000 | 100 | 500 | 1000 |
| $1\ 000 \times 10^3$ | 1.04 | 2.04 | 5.15 | 36.20 | 64.80 | 62.80 |
| 1.000×10^5 | 1.04 | 2.04 | 5.21 | 3.92 | 5.17 | 6.40 |
| 5.000×10^5 | 1.16 | 4.54 | 11.40 | 1.84 | 2.35 | 2.85 |
| 5.348×10^5 | 3.64 | 5.80 | 156.0 | 1.79 | 2.28 | 2.78 |
| 6.000×10^5 | - | -0.97 | -6.17 | 1.15 | 1.16 | 5.28 |
| 1.000×10^6 | - | - | -0.52 | 1.14 | 1.62 | 4.20 |

where $X = 1 (N_c)$, increases at first with increasing collisions and is largest at $\nu_c (5.348 \times 10^5 \text{-sec}^{-1})$. This "bump" is more predominate at the higher frequencies, as shown in the Table. The blank blocks represent cases where the results were not reliable because of an overflow in the computer.

The value of μ' is always greater than unity for all values of ν less than ν_c and is approximately equal for values of ν less than 10^4-sec^{-1} , with the exception of very near the reflection point N_y . N_y is the value of electron density which makes $X = 1 + Y$. The values of μ' near N_y are reduced by increasing the collision frequency as shown in Table 1. This decrease, in turn, is approximately equal to the increase of μ' at $X = 1$.

4. INFLUENCE OF COLLISIONS ON VIRTUAL HEIGHTS

4.1 Method of Obtaining Virtual Heights

The group refractive indices presented in the previous Chapter illustrated the influence of collisions upon these indices. However, the precise effect that is produced upon group heights can only be determined if the ionospheric model is specified. This chapter considers several model shapes whose parameters represent realistic ionospheres and presents the results of group computations made with and without collisions. The results, as will be seen, are quite interesting.

Ray theory, as discussed in Chapter 2, was applied to find the virtual heights presented in this chapter. Since, in Chapter 3, ray theory with collisions was found to be inapplicable to the ordinary mode, only the extraordinary mode need be investigated. In the computation of the virtual heights, μ' was integrated almost up to the classical reflection level where $X = 1 + Y$. This was necessary in that μ' becomes infinite at this level for the zero collision case. However, several tests have shown that, after the upper limit exceeded a certain value, no significant change in the group heights occurred.

It is the aim of this chapter to determine the importance of collisions on virtual heights obtained from several realistic ionospheric models. Virtual heights are tabulated which take into account collisions and are

compared to the same model for which collisions were neglected.

Figure 12 shows the collision frequency model of Nicolet (1963) used in the computations. These values are accurate only to a height of 126 km. Above this height, the collision frequency is difficult to determine because of seasonal and diurnal changes. However, in any case, ν is small and was approximated by a constant value of 10^3-sec^{-1} . This is not a strictly valid approximation, but it was shown in Chapter 3 that the group refractive index for the extraordinary mode is approximately equal for all values of ν less than 10^4-sec^{-1} . Hence, for heights above 126 km, ν was assumed to be 10^3-sec^{-1} .

Five different model shapes were examined; these models, with the equation defining the plasma frequency, f_n , are given below:

Linear: $f_n^2 = \alpha(h-h_b)$

Exponential: $f_n^2 = (VA)^2 \exp(\alpha h)$

where $VA = \exp(\alpha h_b)$

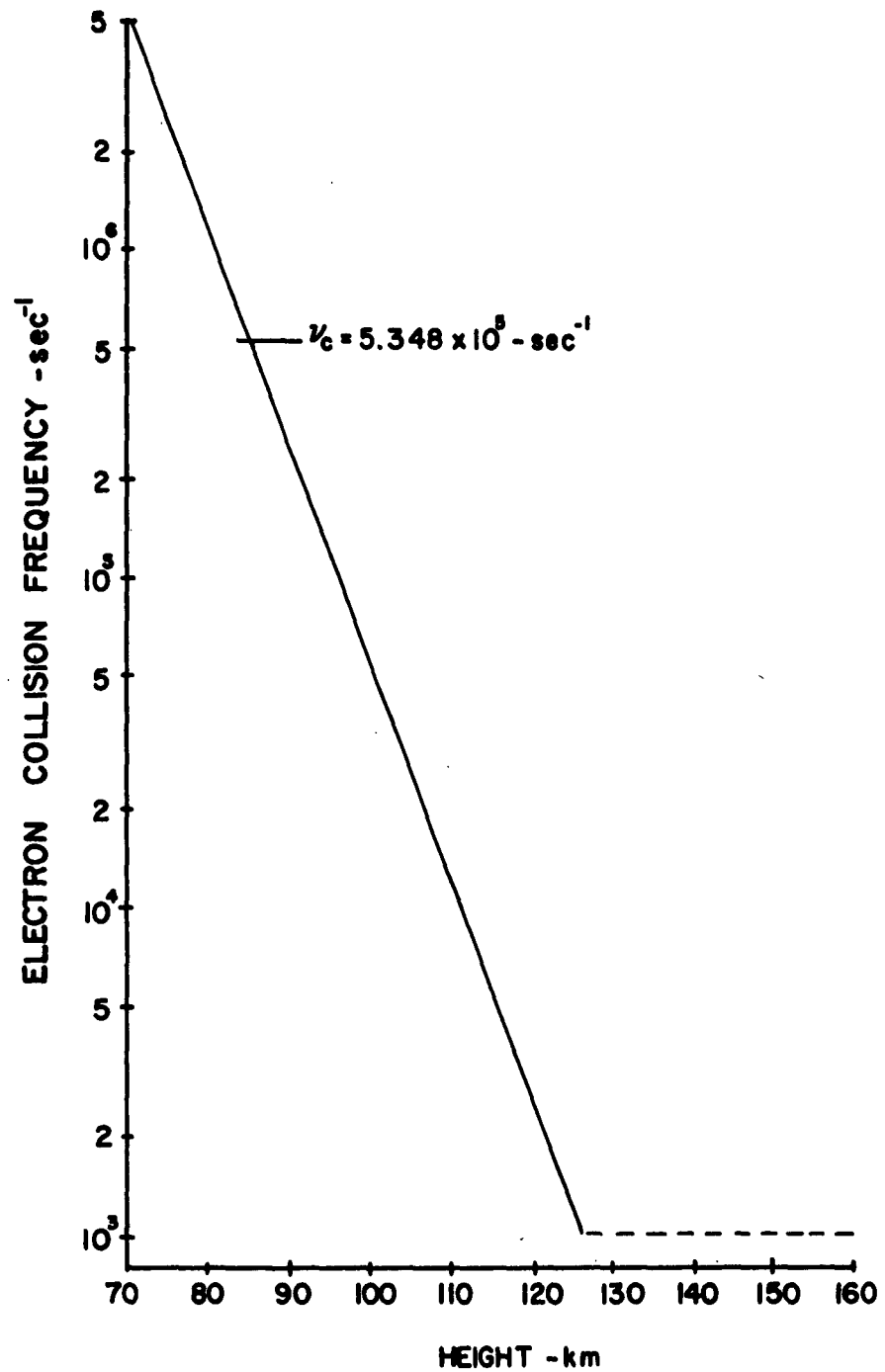
Parabolic: $f_n^2 = f_p^2 \left[1 - \left(\frac{h-h_m}{A} \right)^2 \right]$

where $f_p = \sqrt{80.6179 N_m}$

Cosine: $f_n^2 = \frac{1}{2} f_p^2 \left[1 + \cos \left(\pi \frac{h-h_m}{A} \right) \right]$

Double Cosine: $f_n^2 = \frac{1}{2} f_{p1}^2 \left[1 + \cos \left(\pi \frac{h-h_b}{A} \right) \right] \quad \text{if } f \leq f_{p1}$

or if $f > f_{p1}$: $f_n^2 = \frac{f_{p1}^2 + f_{p2}^2}{2} + \frac{f_{p2}^2 - f_{p1}^2}{2} \cos \left(\pi \frac{h-h_m}{A} \right)$



COLLISION FREQUENCY VS. HEIGHT

FIGURE 12

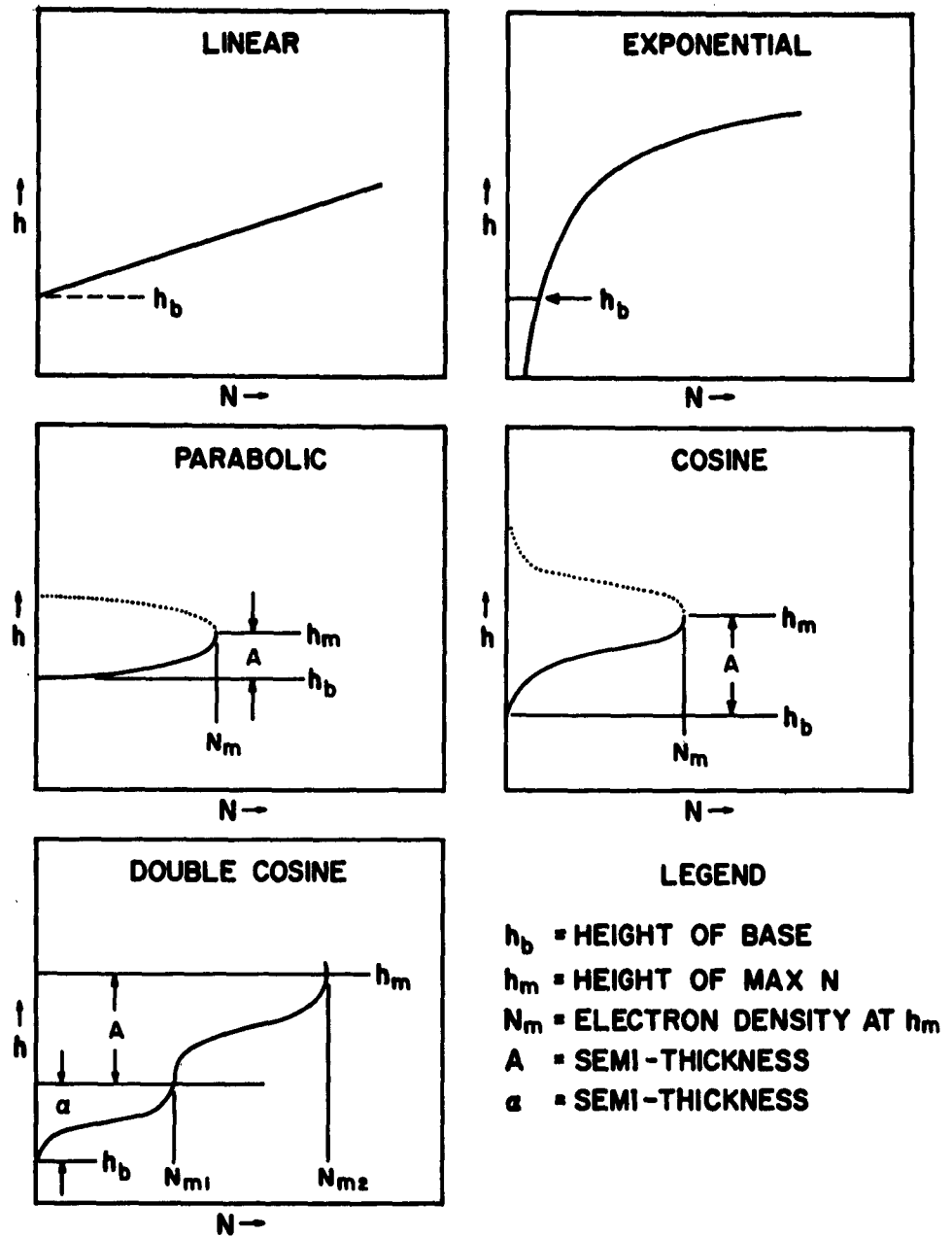
In the above equations, the electron density distribution is readily found, in that f_n^2 is directly proportional to the electron density. The peak of the layer is specified in terms of the penetration frequency, f_p , of the layer for the ordinary mode and is related to the layer maximum electron density, N_m , by $f_p = \sqrt{80.6179 N_m}$.

The N-h profile of each model is shown in Figure 13 and makes clearer the meaning of the parameters given above. The corresponding sketches of typical virtual heights from these models are illustrated in Figure 14.

4.2 Presentation of Tables Showing the Influence of Collisions on Virtual Height

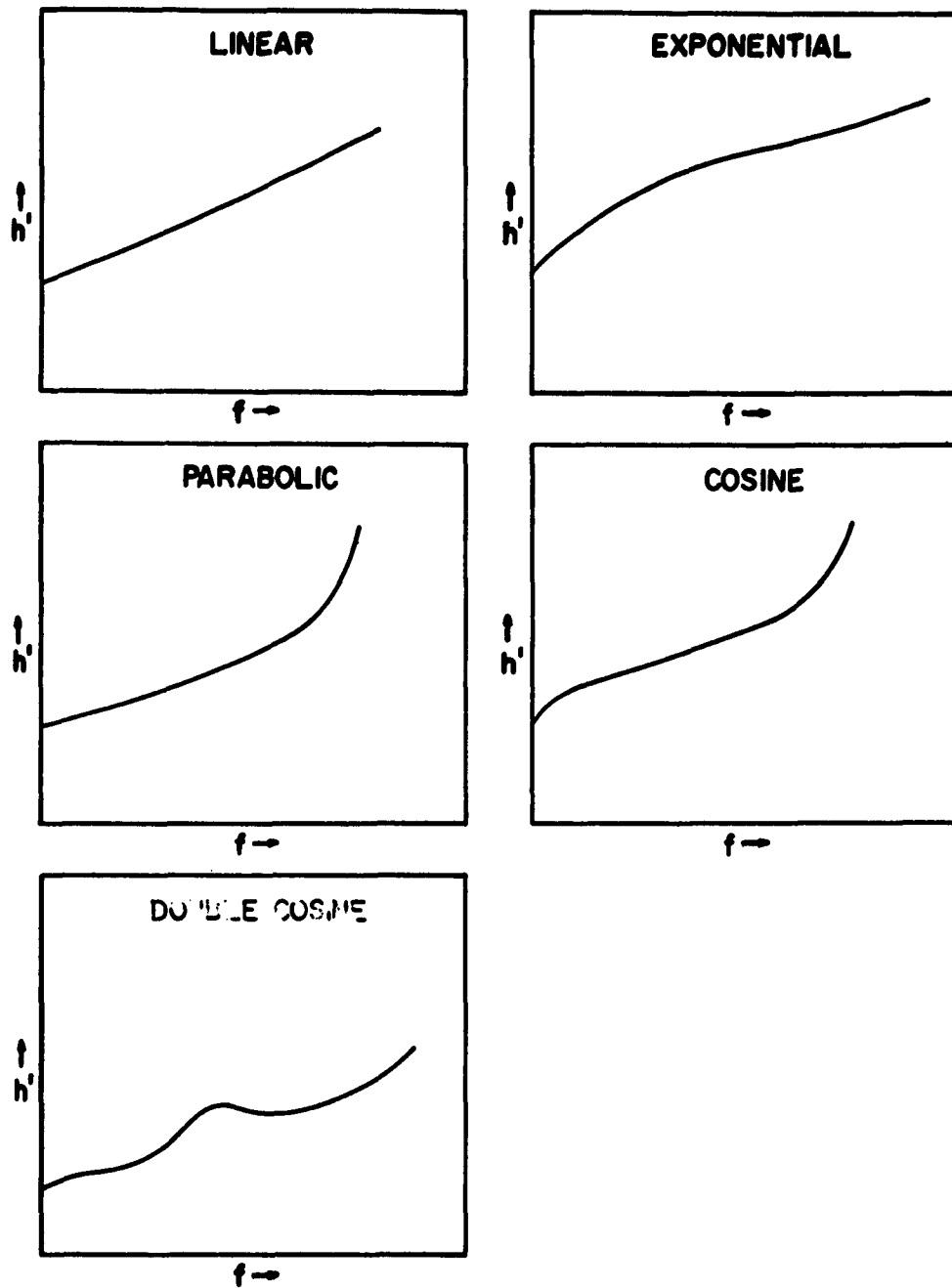
The Tables presented in this section show a comparison between the virtual heights ($h'f$) computed when collisions were considered and the virtual heights ($h'f_0$) computed when collisions were neglected. The percentage error produced by neglecting collisions and the true height of reflection ($h-f$) are also shown. In examining these errors, it should be kept in mind that virtual heights cannot be scaled from records taken at the Ionosphere Research Laboratory to better than ± 7 km.

Many different variations of each model were examined but only selected ones which best illustrate the influence of collisions will be presented. Since the cosine and double cosine models are the most realistic models, more of these have been presented.



N-h PROFILE OF MODELS STUDIED

FIGURE 13



TYPICAL VIRTUAL HEIGHTS FROM MODELS STUDIED

FIGURE 14

TABLE 2

Comparison of Virtual Heights - Linear Models

| Freq (kc/s) | Model A | | | | Model B | | | |
|----------------|-----------------------|----------------------|--------------------------|----------------------|----------------------|----------------------|--------------------------|------------|
| | h-f (km) | h'f (km) | h'f _o (km) | Error % | h-f (km) | h'f (km) | h'f _o (km) | Error % |
| 100 | 87 | 98.4 | 108.1 | 9.6* | 105 | 124.4 | 124.6 | 0.2 |
| 200 | 93 | 133.3 | 139.7 | 4.6* | 111 | 154.3 | 154.3 | - |
| 300 | 100 | 172.9 | 177.4 | 2.5* | 177 | 189.8 | 189.8 | - |
| 400 | 107 | 221.6 | 221.9 | 0.1 | 124 | 231.7 | 231.7 | - |
| 500 | 115 | 274.0 | 273.9 | - | 131 | 280.6 | 280.6 | - |
| 600 | 124 | 334.4 | 334.4 | - | 139 | 337.5 | 337.5 | - |
| 700 | 133 | 404.2 | 404.2 | - | 148 | 403.2 | 403.2 | - |
| 800 | 143 | 484.7 | 484.8 | - | 157 | 478.9 | 478.9 | - |
| 900 | 153 | 578.1 | 578.1 | - | 167 | 566.5 | 566.5 | - |
| 1000 | 165 | 686.6 | 686.6 | - | 178 | 669.1 | 669.1 | - |
| | Model C | | | | Model D | | | |
| | h-f (km) | h'f (km) | h'f _o (km) | Error % | h-f (km) | h'f (km) | h'f _o (km) | Error % |
| 100 | 85 | 85.3 | 104.6 | 18.4* | 93 | 102.1 | 103.1 | 1.0 |
| 200 | 91 | 122.5 | 134.4 | 8.9* | 96 | 117.5 | 119.0 | 1.3 |
| 300 | 97 | 162.5 | 169.8 | 4.3* | 99 | 136.6 | 137.9 | 0.9 |
| 400 | 104 | 208.4 | 211.7 | 1.6* | 103 | 159.5 | 160.2 | 0.4 |
| 500 | 111 | 260.9 | 260.6 | -0.1 | 107 | 186.0 | 186.3 | 0.2 |
| 600 | 119 | 317.6 | 317.5 | - | 111 | 216.6 | 215.7 | - |
| 700 | 128 | 383.2 | 383.2 | - | 116 | 251.7 | 251.7 | - |
| 800 | 137 | 558.8 | 558.9 | - | 121 | 292.1 | 292.1 | - |
| 900 | 147 | 546.4 | 546.5 | - | 126 | 338.8 | 338.8 | - |
| 1000 | 158 | 648.8 | 649.1 | - | 132 | 393.5 | 393.5 | - |
| | Model E | | | | Model F | | | |
| | h-f (km) | h'f (km) | h'f _o (km) | Error % | h-f (km) | h'f (km) | h'f _o (km) | Error % |
| 100 | 82 | 82.8 | 93.1 | 11.1* | 72 | 72.8 | 83.1 | 12.4 |
| 200 | 86 | 86.3 | 109.0 | 20.8* | 76 | 76.0 | 99.0 | 23.2 |
| 300 | 89 | 113.7 | 127.9 | 11.1* | 79 | 79.8 | 117.9 | 32.3 |
| 400 | 93 | 139.0 | 150.2 | 7.5* | 83 | 84.6 | 140.2 | 39.7 |
| 500 | 97 | 165.6 | 176.3 | 6.1* | 87 | 98.8 | 166.3 | 40.6* |
| 600 | 101 | 205.2 | 206.7 | 0.7 | 91 | 150.2 | 196.7 | 23.6* |
| 700 | 106 | 241.5 | 241.7 | 0.1 | 96 | 194.0 | 231.7 | 16.3* |
| 800 | 111 | 282.0 | 282.1 | - | 101 | 229.5 | 272.1 | 15.7* |
| 900 | 116 | 328.7 | 328.8 | - | 106 | 275.9 | 318.8 | 13.5* |
| 1000 | 122 | 383.1 | 383.5 | - | 112 | 370.8 | 373.5 | 0.7 |
| Model | A | B | C | D | E | F | | |
| α | 3.02×10^{10} | 3.2×10^{10} | 3.2×10^{10} | 6.0×10^{10} | 6.0×10^{10} | 6.0×10^{10} | | |
| h_b | 82 | 100 | 80 | 90 | 80 | 70 | | |

TABLE 3

Comparison of Virtual Heights - Exponential Models

| Freq (kc/s) | Model A | | | | Model B | | | |
|----------------|-------------|-------------|--------------------------|------------|-------------|-------------|--------------------------|------------|
| | h-f (km) | h'f (km) | h'f _o (km) | Error % | h-f (km) | h'f (km) | h'f _o (km) | Error % |
| 100 | 119 | 260.9 | 267.3 | 2.4 | 106 | 174.9 | 177.7 | 1.5* |
| 200 | 141 | 305.0 | 309.2 | 1.3* | 116 | 192.5 | 192.4 | - |
| 300 | 154 | 331.9 | 333.2 | 0.4 | 122 | 202.5 | 202.6 | - |
| 400 | 164 | 351.8 | 353.1 | 0.4 | 127 | 211.3 | 211.3 | - |
| 500 | 172 | 370.1 | 371.5 | 0.3 | 130 | 219.6 | 219.6 | - |
| 600 | 178 | 388.2 | 389.6 | 0.3 | 133 | 227.7 | 227.7 | - |
| 700 | 184 | 406.7 | 408.3 | 0.6 | 136 | 236.1 | 236.2 | - |
| 800 | 190 | 426.6 | 428.6 | 0.7 | 138 | 245.2 | 245.2 | - |
| 900 | 194 | 449.2 | 451.9 | 0.6 | 140 | 255.8 | 255.8 | - |
| 1000 | 199 | 477.6 | 481.1 | 1.1 | 142 | 268.8 | 268.9 | - |
| | | | | | | | | |
| Freq (kc/s) | Model C | | | | Model D | | | |
| | h-f (km) | h'f (km) | h'f _o (km) | Error % | h-f (km) | h'f (km) | h'f _o (km) | Error % |
| 100 | 89 | 113.9 | 149.2 | 23.8 | 89 | 114.2 | 137.7 | 17.0 |
| 200 | 97 | 150.2 | 169.4 | 6.5 | 97 | 149.9 | 157.8 | 5.0 |
| 300 | 102 | 162.0 | 168.8 | 3.9* | 102 | 162.7 | 168.7 | 3.6* |
| 400 | 106 | 175.7 | 176.0 | 0.3 | 106 | 176.3 | 176.4 | - |
| 500 | 109 | 182.5 | 182.9 | 0.3 | 109 | 183.3 | 183.4 | - |
| 600 | 111 | 189.3 | 189.7 | 0.2 | 111 | 190.1 | 190.2 | - |
| 700 | 113 | 196.3 | 196.8 | 0.2 | 113 | 197.1 | 197.2 | - |
| 800 | 115 | 203.9 | 204.5 | 0.2 | 115 | 204.6 | 204.7 | - |
| 900 | 117 | 212.5 | 213.4 | 0.3 | 117 | 213.2 | 213.3 | - |
| 1000 | 119 | 222.8 | 224.3 | 0.7 | 119 | 223.7 | 223.9 | - |
| | | | | | | | | |
| Freq (kc/s) | Model E | | | | Model F | | | |
| | h-f (km) | h'f (km) | h'f _o (km) | Error % | h-f (km) | h'f (km) | h'f _o (km) | Error % |
| 100 | 82 | 82.6 | 137.3 | 39.9 | 82 | 82.0 | 105.6 | 22.4 |
| 200 | 89 | 118.1 | 147.7 | 20.0 | 89 | 117.7 | 138.3 | 15.1 |
| 300 | 94 | 139.4 | 155.4 | 10.3 | 94 | 140.0 | 151.8 | 13.2 |
| 400 | 97 | 150.7 | 162.1 | 7.1* | 97 | 150.5 | 161.4 | 6.8* |
| 500 | 100 | 167.8 | 168.4 | 0.5* | 100 | 168.1 | 168.4 | 0.3* |
| 600 | 102 | 173.9 | 174.6 | 0.4 | 102 | 174.3 | 174.7 | 0.3 |
| 700 | 104 | 180.3 | 181.1 | 0.4 | 104 | 180.8 | 181.1 | 0.3 |
| 800 | 106 | 187.0 | 188.1 | 0.7 | 106 | 187.7 | 187.9 | 0.2 |
| 900 | 108 | 194.5 | 196.1 | 0.8 | 108 | 195.4 | 195.6 | 0.2 |
| 1000 | 109 | 203.9 | 206.4 | 1.5 | 109 | 204.7 | 205.1 | 0.2 |

| Model | A | B | C | D | E | F |
|----------|--------------------|-------------------|-------------------|-------------------|-------------------|-------------------|
| VA | 5.19×10^4 | 6.7×10^3 | 6.7×10^3 | 6.7×10^3 | 6.7×10^3 | 6.7×10^3 |
| α | 0.0344 | 0.0768 | 0.092 | 0.092 | 0.1 | 0.1 |
| h_b | 80 | 80 | 50 | 80 | 50 | 80 |

TABLE 4

Comparison of Virtual Heights - Parabolic Models

| Freq (kc/s) | Model A | | | | Model B | | | |
|----------------|-------------|-------------|--------------------------|------------|-------------|-------------|--------------------------|------------|
| | h-f (km) | h'f (km) | h'f _o (km) | Error % | h-f (km) | h'f (km) | h'f _o (km) | Error % |
| 100 | 81 | 80.8 | 83.7 | 3.5* | 103 | 114.7 | 114.9 | 0.2 |
| 200 | 82 | 81.8 | 88.4 | 7.5* | 106 | 133.3 | 133.5 | 0.2 |
| 300 | 83 | 83.0 | 94.3 | 12.0* | 110 | 156.3 | 156.5 | 0.1 |
| 400 | 84 | 84.5 | 101.7 | 16.9* | 115 | 184.6 | 184.8 | 0.1 |
| 500 | 85 | 86.5 | 111.8 | 22.6* | 120 | 219.3 | 219.6 | 0.1 |
| 600 | 87 | 97.9 | 122.3 | 20.0* | 126 | 261.8 | 262.2 | 0.2 |
| 700 | 88 | 115.4 | 136.8 | 15.6* | 132 | 314.3 | 314.8 | 0.2 |
| 800 | 90 | 132.2 | 155.7 | 15.0* | 139 | 379.5 | 380.3 | 0.2 |
| 900 | 93 | 148.6 | 181.0 | 17.9* | 148 | 462.3 | 463.1 | 0.2 |
| 1000 | 94 | 193.7 | 217.3 | 10.9* | 157 | 569.0 | 570.4 | 0.2 |
| | Model C | | | | Model D | | | |
| | h-f (km) | h'f (km) | h'f _o (km) | Error % | h-f (km) | h'f (km) | h'f _o (km) | Error % |
| 100 | 101 | 106.1 | 106.2 | 0.1 | 81 | 81.3 | 86.2 | 5.7* |
| 200 | 103 | 113.9 | 114.1 | 0.2 | 83 | 83.0 | 94.1 | 11.8* |
| 300 | 104 | 123.7 | 123.9 | 0.2 | 84 | 85.0 | 103.9 | 18.2* |
| 400 | 106 | 135.9 | 136.1 | 0.2 | 86 | 92.7 | 116.1 | 20.2* |
| 500 | 108 | 151.2 | 151.3 | 0.1 | 88 | 113.9 | 131.4 | 13.3* |
| 600 | 111 | 170.4 | 170.5 | 0.1 | 91 | 134.0 | 150.5 | 11.0* |
| 700 | 114 | 194.7 | 194.7 | - | 94 | 155.9 | 174.7 | 10.8* |
| 800 | 117 | 226.1 | 226.1 | - | 97 | 193.3 | 206.1 | 6.2 |
| 900 | 121 | 268.3 | 268.3 | - | 101 | 246.0 | 248.3 | 0.9 |
| 1000 | 126 | 328.8 | 328.8 | - | 106 | 307.4 | 308.8 | 0.5 |

| Model | h _b (km) | h _m (km) | A (km) | N _m (el/m ³) |
|-------|---------------------|---------------------|--------|-------------------------------------|
| A | 80 | 110 | 30 | 4 x 10 ¹⁰ |
| B | 100 | 250 | 150 | 5 x 10 ¹⁰ |
| C | 100 | 150 | 50 | 4 x 10 ¹⁰ |
| D | 80 | 130 | 50 | 4 x 10 ¹⁰ |

TABLE 5

Comparison of Virtual Heights - Cosine Models

| Freq (kc/s) | Model A | | | | Model B | | | |
|----------------|-------------|-------------|--------------------------|------------|-------------|-------------|--------------------------|------------|
| | h-f (km) | h'f (km) | h'f _o (km) | Error % | h-f (km) | h'f (km) | h'f _o (km) | Error % |
| 100 | 106 | 119.7 | 120.0 | 0.2 | 95 | 128.0 | 130.6 | 2.0* |
| 200 | 109 | 129.7 | 129.8 | 0.1 | 102 | 156.9 | 157.6 | 0.4 |
| 300 | 111 | 139.0 | 139.0 | - | 109 | 182.7 | 183.2 | 0.3 |
| 400 | 113 | 148.1 | 148.1 | - | 114 | 209.2 | 209.8 | 0.3 |
| 500 | 115 | 157.5 | 157.0 | 0.3 | 120 | 237.8 | 238.5 | 0.3 |
| 600 | 117 | 167.3 | 167.3 | - | 125 | 269.5 | 270.3 | 0.3 |
| 700 | 119 | 177.8 | 177.8 | - | 131 | 305.7 | 306.5 | 0.3 |
| 800 | 121 | 189.1 | 189.1 | - | 137 | 347.6 | 348.8 | 0.3 |
| 900 | 122 | 201.6 | 201.6 | - | 143 | 398.5 | 399.5 | 0.2 |
| 1000 | 124 | 215.9 | 216.0 | - | 149 | 461.4 | 463.6 | 0.5 |
| | Model C | | | | Model D | | | |
| | h-f (km) | h'f (km) | h'f _o (km) | Error % | h-f (km) | h'f (km) | h'f _o (km) | Error % |
| 100 | 89 | 104.2 | 109.5 | 4.8* | 77 | 77.9 | 95.3 | 18.3 |
| 200 | 93 | 121.7 | 125.2 | 2.8* | 81 | 81.8 | 108.8 | 24.8 |
| 300 | 97 | 138.7 | 140.2 | 1.1 | 84 | 85.5 | 121.6 | 29.7 |
| 400 | 100 | 154.7 | 155.7 | 0.6 | 87 | 101.8 | 134.9 | 24.5* |
| 500 | 103 | 171.8 | 172.4 | 0.4 | 90 | 125.7 | 149.2 | 15.8* |
| 600 | 106 | 190.4 | 191.0 | 0.3 | 93 | 144.6 | 165.2 | 12.5* |
| 700 | 110 | 211.6 | 212.1 | 0.2 | 95 | 159.3 | 183.3 | 13.1* |
| 800 | 113 | 236.1 | 236.8 | 0.3 | 98 | 203.3 | 204.4 | 0.5 |
| 900 | 117 | 265.8 | 266.4 | 0.2 | 101 | 227.5 | 229.7 | 1.0 |
| 1000 | 120 | 302.4 | 303.7 | 0.4 | 105 | 258.8 | 261.8 | 1.2 |
| | Model E | | | | Model F | | | |
| | h-f (km) | h'f (km) | h'f _o (km) | Error % | h-f (km) | h'f (km) | h'f _o (km) | Error % |
| 100 | 75 | 75.5 | 87.7 | 13.9 | 80 | 80.0 | 102.0 | 21.6 |
| 200 | 78 | 78.2 | 96.9 | 19.3 | 84 | 85.2 | 119.5 | 28.7 |
| 300 | 80 | 80.7 | 105.5 | 23.5 | 88 | 111.9 | 136.7 | 18.1* |
| 400 | 82 | 83.1 | 114.1 | 27.2 | 92 | 138.3 | 155.2 | 10.9* |
| 500 | 84 | 85.6 | 123.2 | 30.5* | 96 | 161.9 | 176.1 | 8.1* |
| 600 | 86 | 88.4 | 132.9 | 33.5* | 100 | 188.3 | 176.1 | 6.3 |
| 700 | 87 | 108.3 | 143.4 | 24.5* | 104 | 231.6 | 231.9 | 0.1 |
| 800 | 89 | 121.8 | 155.1 | 21.5* | 109 | 273.3 | 273.4 | 0.2 |
| 900 | 91 | 129.3 | 168.4 | 23.2* | 115 | 337.3 | 337.9 | 0.2 |
| 1000 | 93 | 128.8 | 184.0 | 30.0* | 125 | 520.8 | 522.0 | 0.2 |

continued next page

TABLE 5 - continued

| Freq (kc/s) | Model G | | | | Model H | | | |
|----------------|-------------|-------------|--------------------------|------------|-------------|-------------|--------------------------|------------|
| | h-f (km) | h'f (km) | h'f _o (km) | Error % | h-f (km) | h'f (km) | h'f _o (km) | Error % |
| 100 | 91 | 93.9 | 94.2 | 0.3 | 82 | 82.5 | 87.9 | 6.2* |
| 200 | 92 | 96.1 | 96.4 | 0.3 | 84 | 83.7 | 92.0 | 9.0* |
| 300 | 92 | 98.1 | 98.6 | 0.5 | 84 | 84.8 | 95.8 | 11.5* |
| 400 | 93 | 100.3 | 100.8 | 0.5 | 85 | 85.9 | 99.5 | 13.7* |
| 500 | 93 | 102.6 | 103.1 | 0.5 | 86 | 90.1 | 103.5 | 13.0* |
| 600 | 94 | 195.2 | 105.8 | 0.6 | 87 | 96.7 | 107.7 | 10.2* |
| 700 | 94 | 108.2 | 108.8 | 0.6 | 88 | 101.4 | 112.2 | 9.6* |
| 800 | 95 | 111.6 | 112.3 | 0.6 | 88 | 104.2 | 117.2 | 11.1* |
| 900 | 95 | 115.8 | 116.5 | 0.6 | 89 | 113.0 | 122.8 | 8.0* |
| 1000 | 95 | 115.8 | 116.5 | 0.6 | 90 | 127.3 | 129.2 | 1.5 |
| Model I | | | | | | | | |
| 50 | 85 | 85.4 | 97.1 | 12.0* | | | | |
| 75 | 86 | 91.8 | 101.7 | 9.7* | | | | |
| 100 | 88 | 98.8 | 106.2 | 7.0* | | | | |
| 200 | 92 | 120.3 | 125.3 | 4.0* | | | | |
| 300 | 97 | 154.4 | 158.4 | 2.5* | | | | |

| Model | h _b (km) | h _m (km) | A (km) | N _m (el/m ³) |
|-------|---------------------|---------------------|--------|-------------------------------------|
| A | 100 | 250 | 150 | 5 x 10 ¹¹ |
| B | 80 | 200 | 120 | 5 x 10 ¹⁰ |
| C | 80 | 150 | 70 | 5 x 10 ¹⁰ |
| D | 70 | 130 | 60 | 5 x 10 ¹⁰ |
| E | 70 | 130 | 60 | 1 x 10 ¹¹ |
| F | 70 | 130 | 60 | 3.15 x 10 ¹⁰ |
| G | 90 | 100 | 10 | 5 x 10 ¹⁰ |
| H | 80 | 111 | 31 | 1.35 x 10 ¹¹ |
| I | 80 | 103 | 23 | 8 x 10 ⁹ |

TABLE 6

Comparison of Virtual Heights - Double Cosine Models

| Freq (kc/s) | Model A | | | | Model B | | | |
|----------------|-------------|-------------|--------------------------|------------|-------------|-------------|--------------------------|------------|
| | h-f (km) | h'f (km) | h'f _o (km) | Error % | h-f (km) | h'f (km) | h'f _o (km) | Error % |
| 100 | 84 | 84.9 | 119.4 | 28.9 | 94 | 126.1 | 129.4 | 2.6* |
| 200 | 93 | 140.9 | 158.5 | 11.1 | 103 | 167.6 | 168.5 | 0.5 |
| 300 | 105 | 251.3 | 261.6 | 3.9* | 115 | 271.1 | 271.6 | 0.2 |
| 400 | 116 | 251.8 | 257.0 | 2.0* | 126 | 266.4 | 267.0 | 0.2 |
| 500 | 119 | 241.8 | 242.3 | 0.2 | 129 | 251.6 | 252.3 | 0.3 |
| 600 | 122 | 243.5 | 244.3 | 0.3 | 132 | 253.5 | 254.3 | 0.3 |
| 700 | 124 | 249.3 | 250.3 | 0.4 | 134 | 259.5 | 260.3 | 0.3 |
| 800 | 127 | 246.6 | 247.9 | 0.5 | 137 | 256.8 | 257.9 | 0.4 |
| 900 | 129 | 254.3 | 255.9 | 0.6 | 139 | 264.7 | 265.9 | 0.5 |
| 1000 | 131 | 276.4 | 278.2 | 0.6 | 141 | 287.0 | 288.2 | 0.4 |
| | Model C | | | | Model D | | | |
| | h-f (km) | h'f (km) | h'f _o (km) | Error % | h-f (km) | h'f (km) | h'f _o (km) | Error % |
| 100 | 101 | 126.5 | 137.0 | 0.4 | 93 | 120.8 | 124.2 | 2.7* |
| 200 | 107 | 156.0 | 156.4 | 0.3 | 100 | 150.8 | 151.8 | 0.7 |
| 300 | 116 | 233.4 | 233.7 | 0.1 | 106 | 183.9 | 184.5 | 0.3 |
| 400 | 126 | 145.4 | 245.9 | 0.3 | 114 | 233.1 | 233.6 | 0.2 |
| 500 | 129 | 236.8 | 237.4 | 0.3 | 129 | 516.7 | 516.7 | - |
| 600 | 132 | 241.2 | 241.9 | 0.3 | 151 | 524.4 | 525.7 | 0.2 |
| 700 | 134 | 249.8 | 250.5 | 0.3 | 160 | 528.5 | 530.0 | 0.3 |
| 800 | 137 | 251.6 | 252.5 | 0.4 | 168 | 558.4 | 559.8 | 0.3 |
| 900 | 139 | 261.0 | 262.1 | 0.4 | 175 | 607.7 | 610.0 | 0.4 |
| 1000 | 141 | 283.4 | 284.0 | 0.2 | 182 | 654.4 | 656.5 | 0.3 |
| | Model E | | | | Model F | | | |
| | h-f (km) | h'f (km) | h'f _o (km) | Error % | h-f (km) | h'f (km) | h'f _o (km) | Error % |
| 100 | 124 | 190.1 | 190.4 | 0.2 | 99 | 119.3 | 120.0 | 0.5 |
| 200 | 156 | 359.8 | 360.6 | 0.2 | 103 | 139.4 | 139.9 | 0.3 |
| 300 | 169 | 355.1 | 356.1 | 0.3 | 108 | 166.0 | 166.4 | 0.3 |
| 400 | 178 | 379.2 | 380.4 | 0.3 | 115 | 230.3 | 230.7 | 0.3 |
| 500 | 187 | 405.6 | 407.0 | 0.4 | 148 | 551.5 | 552.4 | 0.2 |
| 600 | 195 | 435.0 | 436.6 | 0.4 | 164 | 582.1 | 583.4 | 0.2 |
| 700 | 203 | 478.3 | 480.0 | 0.4 | 177 | 638.1 | 639.7 | 0.3 |
| 800 | 212 | 533.7 | 535.7 | 0.4 | 189 | 720.6 | 722.3 | 0.3 |
| 900 | 220 | 603.5 | 605.5 | 0.3 | 201 | 812.0 | 814.3 | 0.3 |
| 1000 | 230 | 692.4 | 695.4 | 0.4 | 213 | 895.7 | 898.8 | 0.4 |

continued next page

TABLE 6 - continued

| Model G | | | | | Model H | | | |
|----------------|-------------|-------------|--------------------------|------------|-------------|-------------|--------------------------|------------|
| Freq (kc/s) | h-f (km) | h'f (km) | h'f _o (km) | Error % | h-f (km) | h'f (km) | h'f _o (km) | Error % |
| 100 | 82 | 82.6 | 111.3 | 25.8* | 105 | 117.6 | 117.7 | 0.1 |
| 200 | 89 | 112.7 | 139.5 | 19.2* | 108 | 128.6 | 128.7 | 0.1 |
| 300 | 96 | 164.1 | 178.8 | 7.9* | 111 | 141.6 | 141.8 | 0.2 |
| 400 | 109 | 373.0 | 387.4 | 3.6* | 113 | 161.2 | 161.4 | 0.1 |
| 500 | 140 | 532.5 | 533.0 | 0.1 | 120 | 274.7 | 274.7 | 0.1 |
| 600 | 153 | 558.3 | 559.4 | 0.2 | 145 | 487.4 | 488.1 | 0.1 |
| 700 | 165 | 610.2 | 612.4 | 0.3 | 157 | 516.7 | 518.1 | 0.3 |
| 800 | 176 | 687.5 | 690.0 | 0.4 | 166 | 563.2 | 564.7 | 0.3 |
| 900 | 187 | 761.0 | 763.9 | 0.2 | 175 | 630.5 | 632.0 | 0.2 |
| 1000 | 198 | 830.5 | 834.3 | 0.3 | 183 | 704.4 | 706.2 | 0.3 |

| Model | h _b (km) | h _m (km) | α (km) | A(km) | N _{m1} (el/m ³) | N _{m2} (el/m ³) |
|-------|---------------------|---------------------|--------|-------|--------------------------------------|--------------------------------------|
| A | 70 | 150 | 40 | 40 | 7.0 x 10 ⁹ | 5.0 x 10 ¹⁰ |
| B | 80 | 160 | 40 | 40 | 7.0 x 10 ⁹ | 5.0 x 10 ¹⁰ |
| C | 90 | 160 | 30 | 40 | 7.0 x 10 ⁹ | 5.0 x 10 ¹⁰ |
| D | 80 | 300 | 50 | 170 | 1.238x10 ¹⁰ | 1.0 x 10 ¹¹ |
| E | 100 | 300 | 40 | 160 | 3.101x10 ⁹ | 5.0 x 10 ¹⁰ |
| F | 90 | 300 | 30 | 180 | 1.0 x 10 ¹⁰ | 5.0 x 10 ¹⁰ |
| G | 70 | 280 | 40 | 170 | 9.415x10 ⁹ | 5.0 x 10 ¹⁰ |
| H | 100 | 300 | 20 | 180 | 1.238x10 ¹⁰ | 8.0 x 10 ¹⁰ |

The cosine models H and I correspond to day and nighttime models, respectfully, as fitted to data from rocket measurements reported by Smith (1962). Cosine model H is also very similar to a modified Chapman model used by Nertney (1953). Cosine model G corresponds to a sporadic-E layer of thickness 20 km. The linear model A approximates a nighttime model of the lower ionosphere proposed by Mechtly (1962), while the remaining linear models were chosen to illustrate the effect of raising or lowering the base of the ionosphere. The double cosine models approximate the E and F-regions.

4.3 Importance of Collisions

In all models investigated, the errors produced when collisions were neglected were highest when the true height of reflection ($h-f$) was less than 90 km, which is in the height range corresponding to ν_c . This large error, which was independent of model shape, can be accounted for in two ways: (1) The level at which $X = 1$ is in the same range as the height which corresponds to ν_c . This can give rise to negative μ primes as was shown in Chapter 3 and it is here where ray theory should be avoided. (2) The height of reflection is low enough so that the $X = 1$ level is below that range where the collision frequency can cause negative μ primes; in this region μ' is quite small. Whenever collisions are neglected, μ' at reflection becomes infinite; hence, this will produce virtual heights which

are much larger than those produced from case (2). This situation can sometimes be detected by observing whether or not there is much group retardation. If the virtual height (with collisions) is nearly equal to the true height of reflection, as for an example the linear model F or the cosine model E, then one can say that the error produced was that of case (2).

The frequencies which apply to case (1) are marked in the Tables by an asterisk and these virtual heights should be discarded because, as stated in the previous chapter, a negative μ' corresponds to a breakdown of ray theory.

Referring to the linear models, it is noted that the largest errors are produced for those models for which α is the largest. The slope of the profile is determined by α ; larger α 's give rise to a flatter profile. Observing linear models C and E, it will be noted that E produces the larger error. This is because the higher frequencies are reflected at lower levels which are in the "coupling region". For all linear models considered with their base beginning above 90 km, the error produced by assuming zero collisions is negligible. Actually, the base could be extended to 87 km without introducing larger errors since v_c occurs at a height of about 86 km.

The α in the exponential models has a similar effect on the virtual heights. One particular frequency would be reflected lower for a larger α , with all other parameters remaining constant, and in turn would give rise to a larger

error, as shown by the exponential models C and E. The exponential model has a "tail" which would approximate the daytime lower ionosphere.

The parabolic models approximate the nighttime conditions, in that they have no slowly-decaying tail of ionization. Models A and D produce serious errors in parts or all the frequency range examined. The asterisks by each frequency indicate that the $X = 1$ reflection level was in the "critical coupling" region. The higher frequencies were reflected at lower heights because of the large gradients produced by this type of layer. Models B and C with bases at 100 km, produced negligible error when collisions were neglected.

Cosine models D, E, and F are the same model with the exception of the maximum electron density at the peak of the layer. The higher N_m is, the lower the reflection height becomes because of the increased electron density gradients. This, in turn, produces larger errors for a given frequency. The cosine model G which approximates a sporadic-E layer produced small errors when collisions were neglected. Again, as in the previous models, the asterisk refers to those values which are not accurate or reliable because the ray theory cannot be applied in this region.

As illustrated in Figure 14, the double cosine layer can give rise to a "bump" in the group height and this is evident in the double cosine models A, B, C, and E.

This bump is not seen on the models D, F, G, and H since finer frequency intervals would be needed. As previously mentioned, this bump occurs around a frequency which has the $X = 1$ reflection condition at or near the peak of the lower layer, which is sometimes referred to as a "ledge".

From the above observations one can generally tell, given an N-h profile, to which frequencies ray theory (assuming zero collisions) can be applied. However, given the virtual heights from a record, determining the cases which can be reduced by the simplified ray theory is not as straight-forward and simple.

The small margin of errors produced in the virtual heights which are from reflections from the upper layer of the double cosine validates the generally made assumption that the influence of collisions may be neglected in the F-region and at high frequencies. This assumption can be extended to frequencies below 1 mc/s; in fact, this assumption can be extended to almost all low frequency ionograms displaying traces with large group retardations. Sporadic-E layers, which, in general, give rise to an almost flat linear trace, can be reduced by the simplified ray theory method, provided the base of the layer is above 90 km as is usually the case.

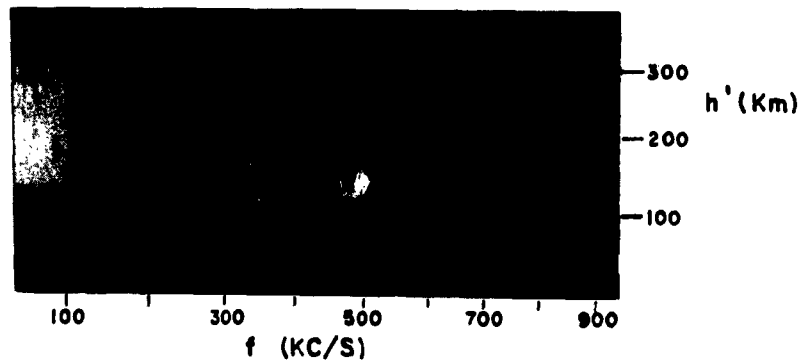
The very low frequency virtual heights (below 300 kc/s) are almost certain to be in error when collisions are neglected; however, when these reflections come from a region above 90 km, the simplified ray theory case can be applied.

5. PRESENTATION OF TYPICAL RECORDS FOR WHICH RAY THEORY CAN BE APPLIED

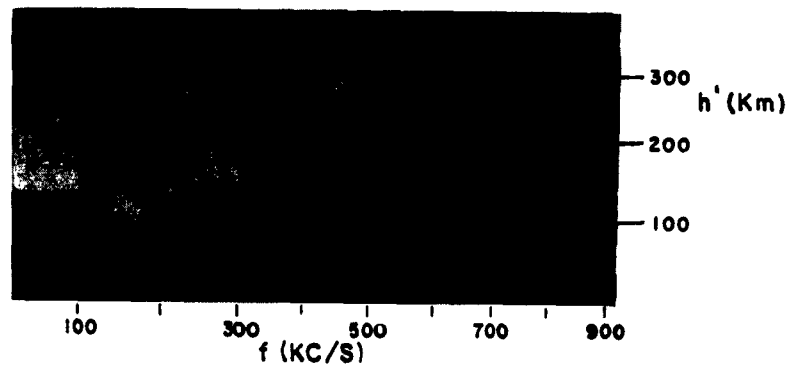
5.1 Presentation of Typical Low Frequency Ionograms

The previous chapter has been concerned with the determination of the theoretical ionogram from a given ionospheric model. In this chapter typical ionograms taken at the Ionosphere Research Laboratory are presented, for which a ray theory treatment of analysis would be possible. It should be pointed out that the usual ionogram corresponds to a situation in which no significant group retardation is observed over the sweep frequency range. This corresponds to reflections from the very steep base of the ionosphere or reflections from the so-called sporadic-E layer. In these cases, only a full wave treatment would be meaningful. However, under certain ionospheric conditions, the features of the upper regions of the ionosphere can be observed, and, at these times, large group retardations are the case, as illustrated by the records given in Figures 15 and 16. Such records are not plentiful, but are frequent enough to justify the objectives of this investigation.

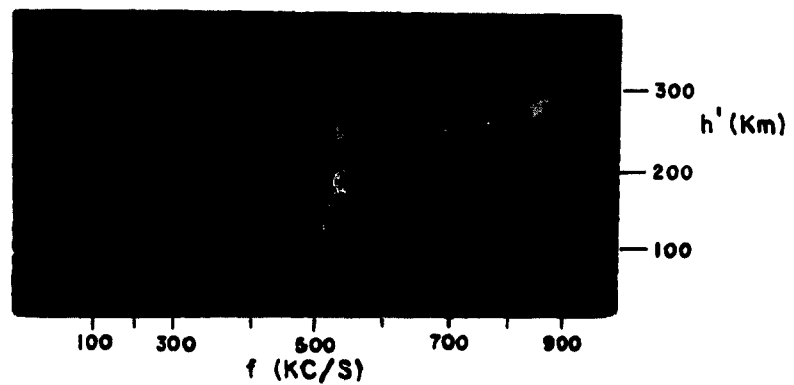
The two specific types which are illustrated are the more frequent forms observed. One, having a region of large group retardation, occurs at about 550 kc/s and corresponds to a sort of double cosine profile, which was discussed in the previous chapter. In this situation, the large group



0523 JANUARY 20, 1963



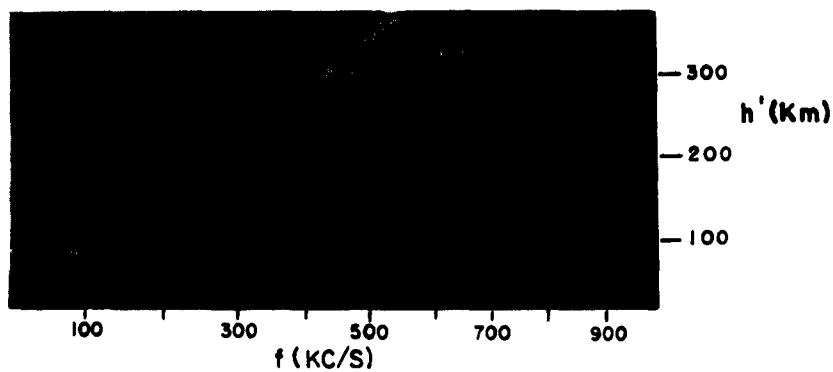
0338 JANUARY 21, 1963



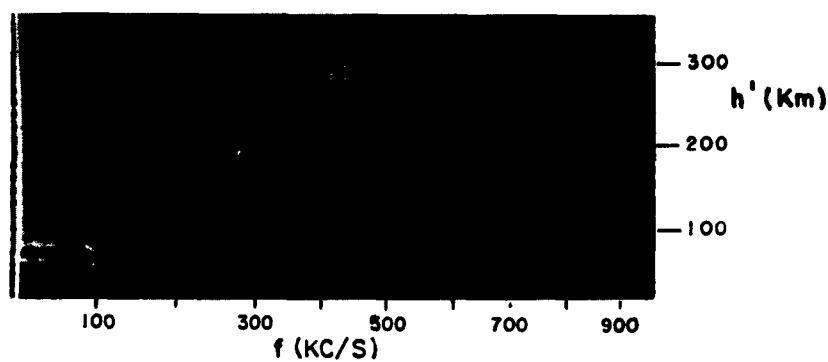
1945 FEBRUARY 9, 1963

EXAMPLES OF RECORDS WITH LARGE GROUP RETARDATIONS

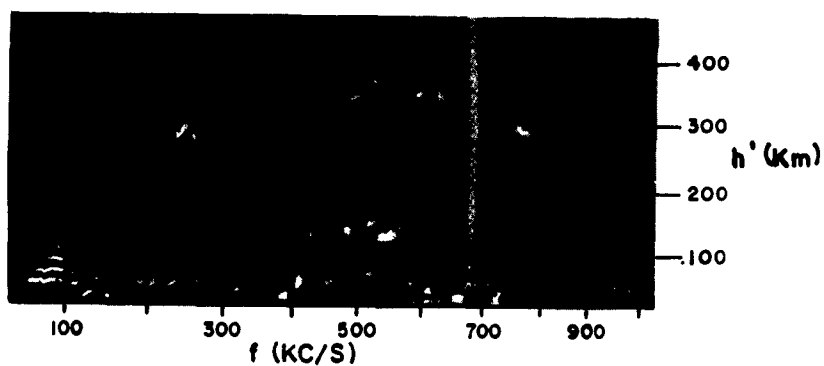
FIGURE 15



0945 JANUARY 29, 1963



1015 JANUARY 29, 1963



2127 AUGUST 7, 1962

EXAMPLES OF RECORDS WITH LARGE GROUP RETARDATIONS

FIGURE 16

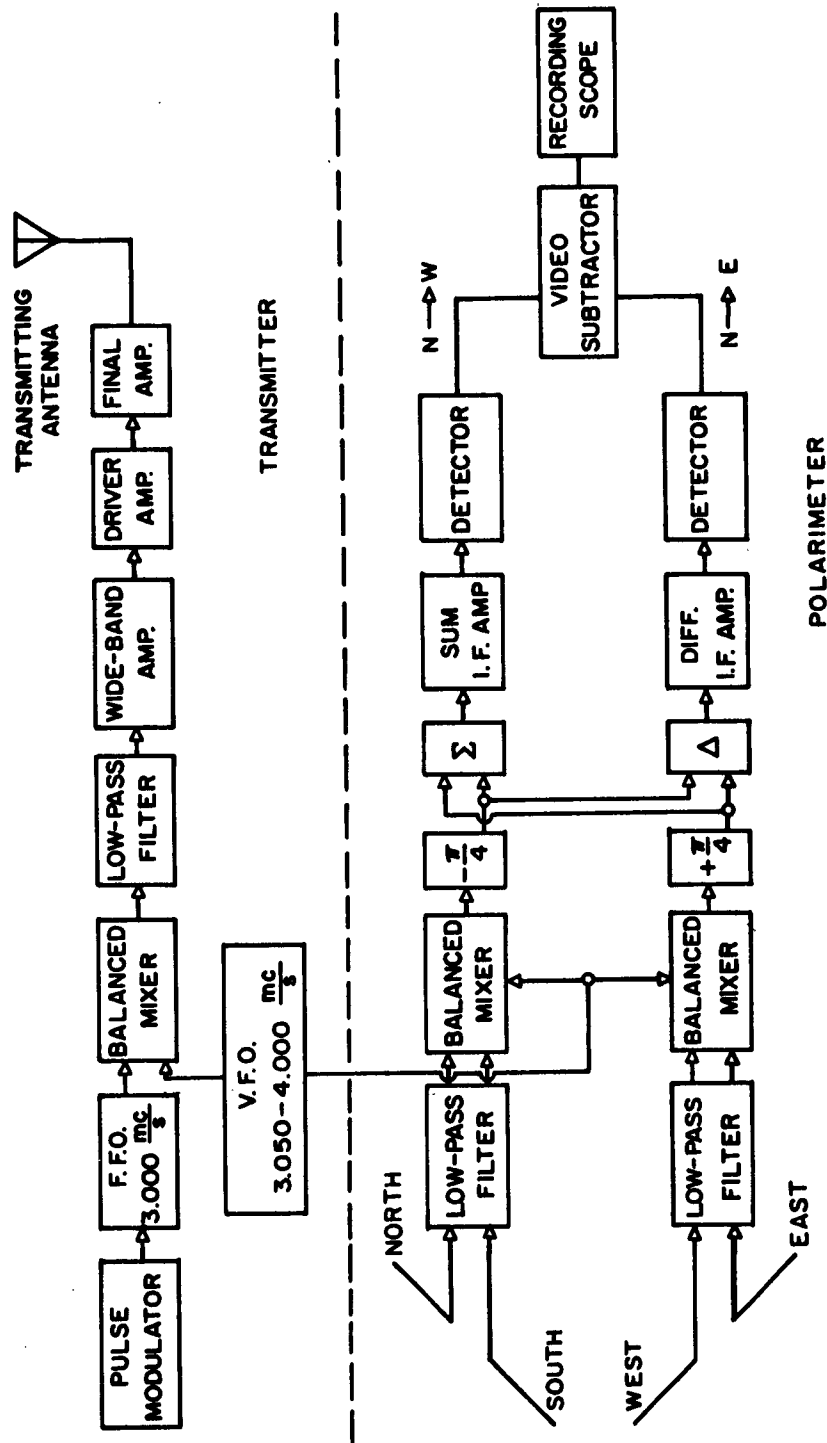
retardation will occur whenever the ionospheric "ledge" becomes $X = 1$ for the extraordinary mode. The other form is simply due to a monotonically increasing electron density distribution like the linear, or exponential models, for instance, also discussed in Chapter 4.

On the records which are presented, it is noted that both light and dark traces are present; these correspond to echoes having North into West and North into East polarization senses respectively, and are purposely so recorded by the polarized receiver in order to distinguish between the two ionospheric modes. Several other interesting ionograms have been catalogued and are given by Hardy (1963).

5.2 Brief Description of the Low Frequency Ionosonde

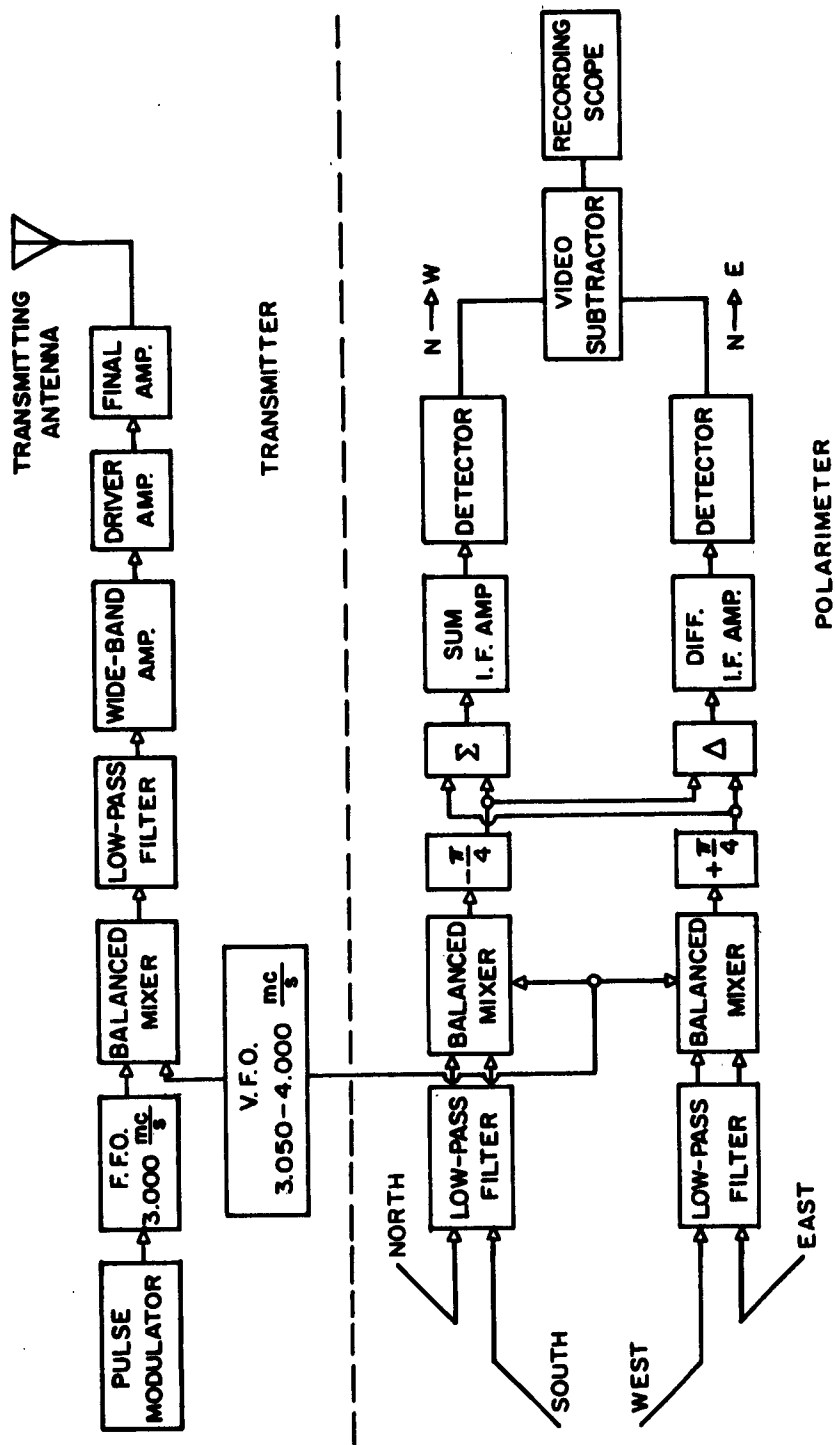
Figure 17 is a block diagram of the transmitting and receiving system which has been used for taking low frequency ionograms. Receiver tracking is accomplished by using the variable frequency oscillator (VFO) of the transmitter as a local oscillator for the receiver to produce a 3 mc/s intermediate frequency. The receiver and recording equipment, inter-connected by cables in order to secure the necessary synchronization between the units, are located 1500 feet from the transmitter.

The polarized receiving antenna consists of two center-fed, co-planar horizontal dipoles at right angles, which are 480 feet long and 90 feet above the ground. Using the



EQUIPMENT BLOCK DIAGRAM

FIGURE 17



EQUIPMENT BLOCK DIAGRAM

FIGURE 17

Parkinson technique, the phase of the signal from one dipole, after amplification is advanced by $\pi/4$, and that of the other dipole retarded by the same amount, so that upon adding these signals a receiver output voltage representing that circular component rotating North into West is produced. Subtraction results in a voltage corresponding to the North into East circular component. This can be made clearer by considering a circularly polarized wave rotating North into West and incident vertically on the antenna. The voltages induced in the North and West legs of the dipole are equal in magnitude, but that in the North leg will be leading by $\pi/2$. If the North voltage is shifted in phase by $-\pi/4$, and that in the West leg by $+\pi/4$, the resulting voltage, when added, will give an output of which the intensity is proportional to the amplitude of the North into West wave. In the N-E channel these voltages are subtracted, and, since they are equal, the resultant produces zero output. In a like manner a North into East wave produces as output in the N-E channel and cancellation in the N-W channel. However, due to equipment characteristics, this cancellation is never complete. The ratio of the voltage produced in the desired channel to that in the rejected channel, which is called the rejection ratio, can be maintained at a value of only 15:1.

In the transmitter, a crystal-controlled 3 mc/s pulsed oscillator is mixed with the VFO, which varies in frequency from 3.050 to 4.000 mc/s. The output of the mixer is

filtered as to allow only the frequencies 50 to 1000 kc/s to drive a wide band amplifier whose 1/2 megawatt peak output is fed into a wide band traveling wave antenna. The sweeping time from 50 to 1000 kc/s can be adjusted in steps of one, two, or four minutes. The records shown in this chapter were obtained from a two minute sweep.

The two outputs from the polarimeter go to a video subtractor-amplifier whose output intensity modulates the Z-axis of an oscilloscope. The quiescent intensity is adjusted for a density on the film of about one-half maximum, so that a decrease in the film density (light) then implies one sense of rotation, and an increased density (dark) corresponds to the other sense of rotation.

All recording is done on 35mm film, and the necessary frequency and height markers along with date markers are automatically photographed.

6. SUMMARY AND CONCLUSIONS

6.1 Statement of the Problem

Ray theory without collisions, which has been successfully used to convert high frequency h'f data into electron density profiles, might be extended to the lower frequencies if the influence of collisions at the lower frequencies are known. The specific aims of this investigation have been to investigate the effect of collisions on low frequency group heights for several realistic ionospheric models and to evaluate the results in order to determine what limitations must be placed upon the frequency and model shapes, if any, so that the simplified ray theory could be applied.

6.2 Review of the Procedure

The investigation procedure involved two phases. In the first, μ' was investigated as a function of sounding frequency, electron density, and collision frequency; the cases corresponding to μ' less than one or negative were ruled out for the application of ray theory. In the second, virtual heights were computed for realistic models with collisions neglected and collisions included and were compared. By noting the error produced and applying the results of the first part of the investigation, cases where ray theory could not be applied were clearly defined.

6.3 Conclusions

As a result of this investigation, the following conclusions can be stated:

- (1) The ordinary mode μ' becomes negative near the reflection point for that mode when collisions are included.
- (2) The extraordinary mode μ' can be negative near $X = 1$ for values of ν at and slightly above ν_c . For values of ν below ν_c , μ' can become large (positive) at $X = 1$. This phenomenon has been neglected by other low-frequency workers.
- (3) The extraordinary mode μ' at the reflection point is controlled by ν ; increasing ν tends to decrease μ' .
- (4) The reduction of the ordinary mode virtual heights at low frequencies by ray theory is not possible.
- (5) The reduction of the extraordinary mode virtual heights by ray theory is not possible under certain restricted conditions. These are:
 - (a) The level at which $X = 1$ is in the same range as the height which corresponds to ν_c ; this can give rise to negative μ' primes.
 - (b) The height of reflection is low enough so that the $X = 1$ level is below that height range where the collision frequency can cause negative μ' primes; in this region μ' is quite small because of the large number of collisions.

- (6) The models displaying sharper gradients produce the greatest error.
- (7) Ray theory can be applied to models having bases starting above 90 km.
- (8) Virtual heights from daytime models can be in error over almost the entire sweep frequency range of interest.
- (9) Sporadic layers may be reduced by ray theory if their base begins above 90 km.
- (10) Nighttime models with a low base (80 km) may possibly be good at frequencies above 300 kc/s.
- (11) Low frequencies reflected from the F-region can always be reduced by ray theory and such ionograms are frequently obtained.

From the above conclusions one can define precisely those N-h models for which ray theory is applicable. However, given an ionogram, the determination over which frequencies the virtual heights can be reduced by ray theory is not straight-forward and simple. From the above conclusions one can be reasonably safe in assuming that zero collision ray theory can be used to reduce virtual heights which exhibit large group retardations; however, one should recompute the virtual heights from the reduced N-h profile including collisions for comparison.

In view of these conclusions, the objectives of this investigation as set forth in Chapter 1 have been satisfied. Observing the limited restrictions as stated above, the re-

duction of low frequency ionograms by ray theory should greatly extend the knowledge of the lower ionosphere.

6.4 Suggestions for Further Study

In order to further the knowledge of the lower ionosphere, the following suggestions are made:

- (1) The development of accurate full wave methods of obtaining virtual heights which could explain the behavior in the regions where ray theory fails.
- (2) The development of ray theory methods for reducing ionograms when collisions are considered.

REFERENCES

- | | | |
|--------------------------------------|-------|--|
| Berning, W. W. | 1950 | Jour. of Meteor., <u>8</u> , 174 |
| Breit, G., and Tuve, M. A. | 1926 | Phys. Rev., <u>28</u> , 554 |
| Brunnschweiler, A. | 1960 | Scientific Report No. 140, Ionosphere Research Laboratory, The Pennsylvania State University |
| Budden, K.G. | 1955 | Phil. Trans. A., <u>248</u> , 45 |
| Budden, K. G. | 1961 | <u>Radio Waves in the Ionosphere</u> , Cambridge University Press |
| Carlson, H. N. | 1960a | Scientific Report No. 129, Ionosphere Research Laboratory, The Pennsylvania State University |
| Carlson, H. N. | 1960b | Scientific Report No. 139, Ionosphere Research Laboratory, The Pennsylvania State University |
| Davids, N. | 1953 | J. Geophys. Res., <u>58</u> , 311 |
| Fejer, J. A. | 1955 | J. Atmosph. Terr. Phys., <u>7</u> , 322 |
| Ferraro, A. J. and Gibbons, J. J. | 1958 | J. Atmosph. Terr. Phys., <u>16</u> , 136 |
| Försterling, K. | 1942 | Hochf. Tech. and Elec., <u>59</u> , 10 |
| Gardner, F.F. and Pawsey, J. L. | 1953 | J. Atmosph. Terr. Phys., <u>3</u> , 121 |
| Gibbons, J.J. and Nertney, R. J. | 1952 | J. Geophys. Res., <u>57</u> , 323 |
| Gibbons, J.J. and Rao, B. R. | 1957 | J. Atmosph. Terr. Phys., <u>11</u> , 151 |
| Hardy, J. D. | 1963 | Scientific Report No. 179, Ionosphere Research Laboratory, The Pennsylvania State University |
| Johler, J. R. | 1962 | Proc IRE, <u>50</u> , 404 |
| Mechtly, E. A. | 1959 | Scientific Report No. 116, Ionosphere Research Laboratory, The Pennsylvania State University |

- Nechtly, E. A. 1962 Scientific Report No. 160,
Ionosphere Research Laboratory,
The Pennsylvania State University
- Nertney, R. J. 1951 J. Atmosph. Terr. Phys., 3, 92
- Nicolet, M. 1963 Manuscript "Aeronomy" to be
Printed in Handbuck Der Physik
- Parkinson, R. W. 1955 Rev. Sci. Inst., 26, 319
- Ratcliffe, J. A. 1958 Magneto-Ionic Theory,
Cambridge University Press
- Rydbeck, O.E.H. 1942 J. App. Phys., 13, 577
- Schmerling, E. R. 1957 Scientific Report No. 94,
Ionosphere Research Laboratory,
The Pennsylvania State University
- Sechrist, C.F., Jr. 1958 Scientific Report No. 103,
Ionosphere Research Laboratory,
The Pennsylvania State University
- Seddon, J. C.,
Pickar, A. D., and
Jackson, J. E. 1954 Jour. Geophys. Res., 59, 377
- Smith, L. G. 1962 Technical Report 62-1-N,
Geophysics Corporation of
America, Bedford, Massachusetts
- Thomas, J. C. 1959 Proc. IRE, 47, 162
- Titheridge, J. E. 1961 J. Atmosph. Terr. Phys., 22, 200
- Watts, J. M. and
Brown, J. N. 1952 National Bureau of Standards
Report 1865, Central Radio
Propagation Laboratory, Boulder,
Colorado
- Waynick, A. H. 1957 Proc IRE, 45, 741

APPENDIX A. DETAILS OF MU PRIME AND VIRTUAL HEIGHT COMPUTATIONS

This section is included in an effort to assist future workers who wish to utilize the techniques presented in this investigation; since the μ' formula is extremely complicated, this appendix presents the μ' formula in a form suitable for computation.

All computations were done on the IBM 7074 digital computer at the Computer Facility of the Pennsylvania State University. The equation for μ' was broken down into shorter equations suitable for programming in the Fortran language utilized with the 7074. A list of these equations based upon the μ' form given in Chapter 3 is:

$$\mu' = UP = U + \frac{F}{2UG^2} \left[-GPP + PGG + \frac{1}{\sqrt{T}} \left(PP(2P-G) + PGG - \frac{2GG}{G}(E^2 + P^2) + 2E(EE) \right) \right] \quad (A-1)$$

where:

$$T = 1 - \frac{4P}{G}(1 - P/G) + (2E/G)^2 \quad (A-2)$$

$$PP(2) = X(PPX - PPY)/F \quad (A-3)$$

$$PP(1) = X(PPX + PPY)/F \quad (A-4)$$

$$PPY = -2A + FAA + 4AX - FXAA + 3ZB - FZBB \quad (A-5)$$

$$PPX = -4 + 16X - 8Z^2 \quad (A-6)$$

$$EE(2) = X(EEY - EEY)/F \quad (A-7)$$

$$EE(1) = X(EEY + EEY)/F \quad (A-8)$$

$$EEY = FXBB - 4XB - FBB + 2B - FZAA + 3ZA \quad (A-9)$$

$$EEX = Z(-14X^2 + 20X - 8 - 10Z - 5YT^2) \quad (A-10)$$

$$GG(2) = 2C(4X + 4Z^2 + 2YT^2 + FAA)/F + 2D(4Z - 6XZ + FBB)/F \quad (A-11)$$

$$GG(1) = 2C(4X + 4Z^2 + 2YT^2 - FAA)/F + 2D(4Z - 6XZ - FBB)/F \quad (A-12)$$

$$AA = YL^2(QAB + Q)/(FA) \quad (A-13)$$

$$BB = YL^2(-QAB + Q)/(FB) \quad (A-14)$$

$$Q = [(AG)QAB + (BG)Z(-10X + 6)]/(CG) \quad (A-15)$$

$$QAB = -YT^4/YL^2 - 2 + 8X - 6X^2 + 4Z^2 \quad (A-16)$$

$$UT = 1/2 - H/2G + W \quad (A-17)$$

IF $UT \geq 0$

$$U = \sqrt{UT} \quad (A-18)$$

$$CHI = |E/UG| \quad (A-19)$$

IF $UT < 0$

$$CHI = [-1/2 + H/2G + W]^{1/2} \quad (A-20)$$

$$U = |E/CHIG| \quad (A-21)$$

$$W = \frac{1}{2}[(1 - H/G)^2 + (2E/G)^2]^{1/2} \quad (A-22)$$

$$P = H/2 \quad (A-23)$$

$$H = 2CX(1 - X) - 2DXZ \quad (A-24)$$

$$G = C^2 + D^2 \quad (A-25)$$

$$E = DX^2 - DX - CXZ \quad (A-26)$$

$$B = (BG)/2A \quad (A-27)$$

$$D(2) = 2XZ - 4Z - B \quad (A-28)$$

$$D(1) = 2XZ - 4Z + B \quad (A-29)$$

$$C(2) = 2 - 2X - 2Z^2 - YT^2 - A \quad (A-30)$$

$$C(1) = 2 - 2X - 2Z^2 - YT^2 + A \quad (A-31)$$

$$\text{IF } X < 1, \quad A = -\sqrt{(AG + CG)/2} \quad (\text{A-32})$$

$$\text{IF } X = 1, \quad A = \sqrt{AG} \quad (\text{A-33})$$

$$\text{IF } X > 1, \quad A = \sqrt{(AG + CG)/2} \quad (\text{A-34})$$

$$CG = \sqrt{AG^2 + BG^2} \quad (\text{A-35})$$

$$BG = -8YL^2Z(1 - X) \quad (\text{A-36})$$

$$AG = YT^4 + 4YL^2(1 - X)^2 - 4Z^2YL^2 \quad (\text{A-37})$$

$$Z = AK3V/F \quad (\text{A-38})$$

$$YT = AK2(\text{FIELD})\text{SINF}(\text{THETA}AK4)/F \quad (\text{A-39})$$

$$YL = AK2(\text{FIELD})\text{SINF}(\text{THETA}AK4)/F \quad (\text{A-40})$$

$$X = AK1(\text{ELECT})/F^2 \quad (\text{A-41})$$

$$RA = A - AX - BZ \quad (\text{A-42})$$

$$RB = BX - B - AZ \quad (\text{A-43})$$

$$RD = 2YL[(1 - X)^2 + Z^2] \quad (\text{A-44})$$

$$R(1) = (-YT^2Z + RB)/RD \quad (\text{A-45})$$

$$R(2) = (-YT^2Z - RB)/RD \quad (\text{A-46})$$

$$S(1) = (YT^2 - XYT^2 + RA)/RD \quad (\text{A-47})$$

$$S(2) = (YT^2 - XYT^2 - RA)/RD \quad (\text{A-48})$$

$$\text{DELTA} = 10^{10} \left(\left| 1 - [R(1)R(2) - S(1)S(2)] \right| + \left| R(1)S(2) + R(2)S(1) \right| \right) \quad (\text{A-49})$$

$$AK1 = 8.06179 \times 10^1 \quad (\text{A-50})$$

$$AK2 = 2.79938 \times 10^{10} \quad (\text{A-51})$$

$$AK3 = 0.159155 \quad (\text{A-52})$$

$$AK4 = 1.74528 \times 10^{-2} \quad (\text{A-53})$$

Under certain conditions the argument in the square root used in determining μ could become negative (this refers to (A-18)) and an alternate form of computation must be used to solve for μ . Such a situation could occur for

a small number of collisions. If this occurred, x was computed first and μ was found in terms of x through (A-21). This difficulty is handled in the program by the use of "IF" statements. "IF" statements are also used to determine the correct signs for other square roots, as described below, and to bypass certain operations when the zero magnetic field case is to be studied. If this is not done the maximum capacity of the computer would be exceeded. Therefore, the program which was developed is flexible in that the no field case with or without collisions, in addition to the case when all the variables are included, could be employed.

It will be noted in the list of equations that some of the quantities are subscripted with (1) or (2). The subscript (1) corresponds to the plus sign and (2) to the negative sign which appears in front of the square root operation. The plus sign is taken to correspond to the extraordinary mode and the minus to the ordinary mode. However, if the collision frequency is greater than the critical collision and if X is equal to, or greater than one, the opposite signs must be used. This must be done if the μ' curves are to be continuous through the point $X = 1$. This change of sign is done automatically in the program. The following chart would make this convention easy to follow.

| $\nu < \nu_c$ | | | $\nu > \nu_c$ |
|---------------|-----------|--------------|---------------|
| Ext | + | - | + |
| Ord | - | + | - |
| | $N < N_c$ | $N \geq N_c$ | For all N |

The double-lettered quantities are the partial derivatives of the single-letter quantities with respect to the operating frequency. The DELTA or accuracy check (A-50) was included to serve as an indication of the accuracy of the calculation. This should be zero ideally, but values between 10^2 and 10^3 are acceptable. It should be noted that there is a factor of 10^{10} times the actual DELTA introduced for ease of read-out. Near the reflection points where parameters vary rapidly the accuracy check may be 10^4 or higher.

Comparison of the results from this program and a similar program written in double precision has shown agreement to at least six figures, with the exception of the ordinary mode values which agree to three figures near the reflection point $X = 1$. Only the extraordinary mode was considered in the computation for the virtual heights. In this comparison only μ and X values were available from the double precision data. Since errors in the calculation of μ and X were small, it is a reasonable assumption that μ' calculations would not call for double precision computation.

Theta, the magnetic field, the electron density, the collision frequency, and the operating frequency, which make up the parameters, are read in on a data card with no limitations on the number of data cards to be used. On the last data card a number for the variable LAST is read in which stops the program. The computation time required for

each set of parameters is 0.4 second.

In the program to find virtual heights the mu prime program is used as a sub-program. It is actually the integrand of the integration routine. The method used to find virtual heights is that of integrating μ' up to the classical reflection points, e.g., $X = 1$ for the ordinary mode and $X = 1 + Y$ for the extraordinary. The integral used was

$$h'f = \int_{h_b}^{h_r} \mu' dh \quad (A-54)$$

where h_r is the height of reflection and h_b is the height of the base of the layer.

The numerical integration technique used was a Gaussian quadrature method in which an extended five-point Gaussian quadrature formula was used which is exact for ninth-degree polynomials. The formula is accurate to the extent that the integrand can be approximated by a ninth degree polynomial over each five-point segment of each interval.

The number of intervals is specified in the input data. Test have shown that fifteen intervals is sufficient. The difference in the virtual heights computed from fifteen intervals to those with fifty or one-hundred is in the fractions of one percent. Therefore, when fifteen intervals are specified the integration is over 75 height segments.

The method used to determine the true height of reflection is that of solving the plasma frequency equation, which is a specified function of height for a given model, for h

when the plasma frequency f_n is equal to f , the operating frequency, for the ordinary mode, and f_n is equal to $f(1+Y)$ for the extraordinary mode. This is done in a sub-program which must be changed for each different model shape. The height of the base, h_0 , is read in as a constant.

The μ' program had to be modified slightly for use with the virtual height routine. Since μ' was to be integrated over height, X must be known as a function of height. A sub-program was written which would give the plasma frequency as a function of height; and, since $X = f_n^2/f^2$, the value of X is obtained. Any new model can be used if the necessary sub-programs are written. The time required to find one virtual height curve for ten frequencies is approximately 20 seconds.

PSU SN 189

The Pennsylvania State University.

AN INVESTIGATION OF THE INFLUENCE OF COLLISIONS ON

LOW FREQUENCY GROUP HEIGHTS. J. D. Hardy

July 15, 1963. 75p

In this report virtual heights from five different models representing realistic ionospheres are computed. Computations are made including collisions and neglecting collisions, and the results are compared to determine the magnitude of the errors produced when collisions are neglected. Limitations are stated which must be placed upon frequency and model shapes, in order that ray theory may be applied.

Obtainable from IRL, The Pennsylvania State University

PSU SN 189

The Pennsylvania State University.

AN INVESTIGATION OF THE INFLUENCE OF COLLISIONS ON

LOW FREQUENCY GROUP HEIGHTS. J. D. Hardy

July 15, 1963. 75p

In this report virtual heights from five different models representing realistic ionospheres are computed. Computations are made including collisions and neglecting collisions, and the results are compared to determine the magnitude of the errors produced when collisions are neglected. Limitations are stated which must be placed upon frequency and model shapes, in order that ray theory may be applied.

Obtainable from IRL, The Pennsylvania State University

I. J. D. Hardy

II. PSU SN 189

PSU SN 189

The Pennsylvania State University.

AN INVESTIGATION OF THE INFLUENCE OF COLLISIONS ON

LOW FREQUENCY GROUP HEIGHTS. J. D. Hardy

July 15, 1963. 75p

In this report virtual heights from five different models representing realistic ionospheres are computed. Computations are made including collisions and neglecting collisions, and the results are compared to determine the magnitude of the errors produced when collisions are neglected. Limitations are stated which must be placed upon frequency and model shapes, in order that ray theory may be applied.

Obtainable from IRL, The Pennsylvania State University

PSU SN 189

The Pennsylvania State University.

AN INVESTIGATION OF THE INFLUENCE OF COLLISIONS ON

LOW FREQUENCY GROUP HEIGHTS. J. D. Hardy

July 15, 1963. 75p

In this report virtual heights from five different models representing realistic ionospheres are computed. Computations are made including collisions and neglecting collisions, and the results are compared to determine the magnitude of the errors produced when collisions are neglected. Limitations are stated which must be placed upon frequency and model shapes, in order that ray theory may be applied.

Obtainable from IRL, The Pennsylvania State University

I. J. D. Hardy

II. PSU SN 189

I. J. D. Hardy

II. PSU SN 189